

# On the fatigue behaviour and reliability assessment of high strength welded details

*Burak Karabulut<sup>1</sup>, Gonçalo Ferraz<sup>1</sup>, Barbara Rossi<sup>1&2</sup>*

<sup>1</sup> *KU Leuven, Faculty of Engineering Technology, Sint-Katelijne-Waver, Belgium.*

<sup>2</sup> *University of Oxford, Department of Engineering Science, Oxford, United Kingdom.*

## **Abstract**

This research focusses on the fatigue behaviour of welded components made of high strength duplex (EN 1.4162) and carbon steel. It starts by investigating the base material alongside welded cruciform joints submitted to cyclic loading through experiments and finite element models. The obtained results are then compared with existing research on high strength (carbon and stainless) steel equivalents. This collated database of more than 500 reference test results is then used to assess the applicability of the current Eurocode and IIW provisions to predict the fatigue life of higher strength steels and to propose new rules that include the benefit of their higher material strength. Proposals are made to upgrade certain fatigue classes (e.g., transverse stiffeners and butt welds) when high strength steel grades are employed. The reliability of these proposals is then supported by the use Weibull models, commonly used in survival analysis.

## **Keywords**

Fatigue assessment; Duplex stainless steel; High-strength steel; Hot spot stress method; Nominal stress method; Reliability.

## **1 General positioning of the problem**

Since August Wöhler's pioneering discoveries in 1850, a considerable lot of research has been conducted due to the inherent complexity of the mechanisms involved in fatigue failure modes [1], which has ultimately led to a number of design guidelines [2–7]. Because of the inevitable welded details in steel girder bridges, fatigue is frequently thought to be the primary design requirement [6]. However, until a significant number of failures occurred, were examined, and subsequently were linked to fatigue, this phenomenon was underestimated [8,9]. Following that time, research adopted the standardized fatigue resistance curves, also known as SN-curves or Wöhler curves, with the aim

of establishing correlations between the applied stress range ( $S$ ) and the fatigue endurance (number of cycles at failure,  $N$ ) of a variety of typical features.

When it comes to the design of steel structures against fatigue, the European standard EN 1993-1-9 [10] is the most widely used reference. It is applicable to a wide range of materials, including carbon steel grades, stainless steel grades, and weathering steel grades, provided that these grades meet the toughness requirements of EN 1993-1-10 [11]. As presented in the background documentation to the European standard [12], the SN-curves provided in EN 1993-1-9 [10] for different critical fatigue details were mostly derived based on abundant experimental investigations on mild steel components with a nominal yield strength  $f_y$  ranging between 235 and 400 MPa. However, higher strength steel grades are typically found to have higher fatigue strength in the literature [13–24]. Yet, because fatigue design is currently governed by the structural detail category (i.e., its geometry, manufacturing methods, and execution quality), where the mechanical properties of the base material do not play a role, it is not currently possible to benefit from the higher material strength.

Interest in stainless steel in constructions has increased recently because of its great mechanical strength and corrosion resistance the combination of which resulting in lower maintenance costs and longer lifespan [25]. Stainless steel can be classified into four families based on its microstructure: austenitic, martensitic, ferritic, and austenitic-ferritic (duplex). The microstructure of duplex grades is balanced between ferrite and austenite. On the other hand, lean duplex grades, which are duplex grades with a reduced Ni content in mass, such as the grades EN 1.4162 (also designated as UNS S32205 or LDX 2101 in the US), have become more common in the last 20 years due to a much lower initial cost. According to several research [26–29], those grades do in fact exhibit comparable or superior corrosion resistance to austenitic stainless steel grades EN 1.4307 and EN 1.4404. As a result, they are being used in constructions exposed to harsh environmental conditions and cyclic loads, such as coastal bridges.

There is little scientific literature on EN 1.4162 duplex grades because previous studies on the fatigue behaviour of stainless steel welds have largely focused on standard austenitic or duplex grades, such as EN1.4404 and EN1.4462 [8,13,19,24,30–32]. The majority of earlier research on the lean

duplex grades concentrated on describing their material behaviour, such as their fracture toughness, hardness, and surface roughness, as well as the effects of post-weld treatments (PWT) on the microstructure and, consequently, the initiation and growth of fatigue cracks, as reported in [19,31,33,34]. Even though lean duplex stainless steel grades are currently and steadily being used in the construction industry, there is very little research on their fatigue performance at the structural level [25,35]. Additionally, when compared to carbon steel equivalents, duplex welded specimens tend to have different microstructural and mechanical properties, such as a narrower heat affected zone (HAZ), a different residual stress distribution, and geometrical imperfections. However, these differences have not yet been studied or linked to the fatigue behaviour of duplex welded specimens.

In Sections 2.1 and 2.2, fatigue experiments on the base (unwelded) plate as well as on welded cruciform joints built of duplex EN 1.4162 grade were conducted in order to better understand the fatigue behaviour of (lean) duplex grades. In Section 3, a database of reference experimental results that have been compiled for comparable high-strength steel details was presented. In order to gain insight into how the current design rules could be improved to take into account the gain in fatigue life for such higher strength metal grades in bridge applications, the obtained experimental SN-curves are then compared to the current European ones and re-evaluated in accordance with the hot spot stress method. And the reliability of these evaluations in Section 3 is then supported by the use of Weibull models in Section 4, which are commonly used in survival analysis. Finally, conclusions were drawn on the efficiency of current fatigue design rules and possibilities for improvement were discussed and supported by the results of reliability analysis.

## **2 Experimental study**

Through experimental research, the fatigue behaviour of the duplex EN 1.4162 grade is examined in this part. Characterizing the behaviour of the base material as well as welded specimens under static tensile and cyclic fatigue loading is required for this. Transversal stiffeners, or welded cruciform joints, are frequently the most important fatigue-prone element determining the fatigue limit state in orthotropic deck or girder bridges, as noted in [9,36,37], and they are typically unavoidable [38,39]. This detail frequently governs the design in conventional welded girder bridge applications, as was

previously shown in [40]. This is the reason why, in this paper, non load-carrying fillet welds (of transverse attachments onto a base plate) were studied, and the used material grade was the lean duplex.

## 2.1 Mechanical behaviour of base material made of EN 1.4162

### 2.1.1 Measured stress-strain curves of base material

Static tensile tests were carried out on dog-bone coupons to describe the mechanical characteristics of the base plate and the stiffeners. The tested samples contain plates with nominal thicknesses of 12 mm (plate) and 8 mm (stiffener), as will be discussed in Section 2.2.2. Three coupons were taken in the rolling direction (RD) and the transverse direction (TD) to examine anisotropy (RD). As further explained in [40,41], DIC was used to measure the strain field and Match ID to interpret the measured data.

The elasticity modulus  $E$ , according to [42,43], was calculated between 10% and 40% of the proof strength. In fatigue testing, the RD of the test samples corresponds to the loading direction (as described in Section 2.2.2). In the RD, base plates for 12 mm and 8 mm coupons had average values of 202 GPa and 204.33 GPa for the elasticity modulus  $E$ , respectively (see Table 1). Given the low standard deviation ( $Stdv$ ), this result is in good agreement with the nominal values offered for the examined material grade in [42], indicating that the nominal value of  $E$  can be used for computing the HS stress ranges based on measured elastic strains (see Section 2.2.4.2). For the 12 mm and 8 mm base plates respectively, an average value of  $f_y = 502.3$  MPa and 518.3 MPa for the RD was found, which is consistent with the literature [31,44,45].

Table 1 Static tensile test results of the 12 mm and 8 mm base plates made of EN 1.4162 grade [41].

Test specimen	$E$ [GPa]	Average $E$ [GPa]		$Stdv E$ [ $\sigma$ ]		$f_y$ [MPa]	Average $f_y$ [MPa]		$Stdv f_y$ [ $\sigma$ ]	
		12 mm	8 mm	12 mm	8 mm		12 mm	8 mm	12 mm	8 mm
RD1	205	202	204.33	3.61	0.58	502	502.3	518.3	0.58	2.31
RD2	203					502				
RD3	198					503				
TD1	215	211.67	220	3.06	1.00	520	520.3	574.7	0.58	1.53
TD2	209					521				
TD3	211					520				

### 2.1.2 Fatigue test results of the base plates

The fatigue behaviour of base plates built of EN 1.4162 duplex grade was investigated using 17 specimens that were dimensioned in accordance with [46]. Utilizing wire electrical discharge machine

cutting (Wire EDM) technology, highly smooth edges that complied with dimensional tolerances of [43,47,48] were produced. With a frequency of 10 Hz and a stress ratio  $R$  of 0.3, constant amplitude fatigue tests were carried out using the Instron 8802 series servo-hydraulic testing frame. The stress ratio of 0.3 was chosen to comply with the possible worst case scenario since a higher stress ratio implies a higher mean stress that simulates higher residual stresses present in the welded details [49–51]. This was envisaged in order to represent higher residual stresses present in the welded connections for real bridge applications as the experimental samples were of smaller scale.

The results are listed in Table 2, and in Section 2.2.4, a comparison between those findings and the fatigue life of welded samples is made. If fixed slopes for the SN curve are taken into account, the comparison of the detail categories shows a 56 % decrease in fatigue resistance (“BP” for base plates and “welded” for the stiffeners as shown in Fig. 3), emphasizing the significant reduction in fatigue life that can be attributed to the welding process and its associated imperfections (i.e. residual stresses, geometrical misalignment, geometrical discontinuity and stress concentration effect, etc.). The base plates' fatigue class is substantially higher than the IIW's recommended fatigue class of  $FAT_k = 160$  MPa, which is partially attributable to the higher material strength, as they are free of these imperfections (see Table 2).

Table 2 Fatigue strength characteristics of the tested base plate made of EN 1.4162 grade.

SN-curve characteristics (95% fractile)	$FAT_k$ [N/mm <sup>2</sup> ]	$FAT_m$ [N/mm <sup>2</sup> ]	$Stdv$ [ $\sigma$ ]	Coefficient of variation (CoV)	Comparison with fatigue class FAT160 [10]
$m = 5.00$	189.16	252.85	0.294	0.016	+ 18.2%
$m_{var} = 12.43$	295.10	315.31	0.167	0.004	+ 84.4%

## 2.2 Fatigue behaviour of welded specimen made of EN 1.4162 grade

### 2.2.1 Welding parameters and microstructural investigations

Gas metal arc welding (GMAW) with metal active gas was employed to create the fillet welds of the examined detail (MAG). Maintaining the austenitic-ferritic balance of the microstructure is crucial for duplex grades to preserve corrosion and mechanical resistance as well as ductility, hence consideration should be given to microstructural constraints. The primary procedure to preserve the balanced microstructure is to keep the heat input (HI) within the range of 0.5 to 1.5 kJ/mm and to adhere to the inter-pass temperature of 150 °C [52]. Pulse-arc welding was employed to meet the HI limit because

it guarantees good penetration. Respecting these guidelines can reduce the likelihood of intermetallic phase development and prevent excessive ferrite formation in the heat affected zone (HAZ).

Böhler CN 24/9 LDX with 1.0 mm solid wire was used as the filler material. In order to take into account element loss, prevent segregation, and restrict the formation of ferrite in the weld metal (WM), HAZ, and fusion zone (FZ), the proper type of weld metal (i.e., filler, WM) must be chosen. On the pre-production test parts, destructive and non-destructive tests (DT and NDT) were carried out. The welds were examined using NDT techniques for inclusions, cracks on the surface, mismatch, undercut, impurities, and weld convexity. It was intended to reach the highest quality level B in [53], and it was achieved. As further elaborated in a previously published work of current paper's authors, preliminary welded T-joint specimens with various welding parameters were cut, polished, and chemically etched to undergo DTs and NDTs, and a satisfactory microstructure was observed. Further details about the welding parameters and their qualification can be found in [41].

Another crucial finding concerns the size of HAZ size, which is around 0.08 mm and it can be typically up to 20–40 times larger for carbon steel equivalents [54,55]. Hardness tests were also carried out in addition to the microstructural examinations in accordance with [56], and average Vickers hardness (HV10) values of 232 for the BM and 222 for the WM were obtained, both of which are consistent with [42]. According to [44], the hardness difference between BM and WM is comparable enough to predict no appreciable changes in strength, hence no additional micro-hardness measurements in the HAZ were made.

### **2.2.2 Sample preparation and welding sequence**

The dimensions of the tested specimen were selected based on numerical investigations where the influence of geometrical model parameters on the stress concentration factors (SCF) were evaluated in a sensitivity analysis, which was based on earlier published research from the same authors [17,41,57,58]. The results of this sensitivity analysis are described in greater detail in [40]. The main goal was to show the same fatigue life as in [57] by having the examined sample have the same stress concentration factor (SCF) and thus HS stress as that found in a transversal stiffener of a specified bridge girder. Fig. 1 shows the test specimen's dimensions.

The test pieces were cut by Wire EDM as illustrated in Fig. 1(b) after the stiffeners were welded onto a plate (about 400 mm by 200 mm). One large welded plate might yield three to four suitable examples, thus five batches of welded plates were made in order to have roughly fifteen to twenty specimens for fatigue testing, as advised by IIW recommendations for a statistical analysis [51]. The x-axis in Fig. 1(b), which corresponds to the loading direction, is the base plate's RD. This was done in order to prevent any potential improvement in fatigue resistance brought on by the TD's higher mechanical strength (see Table 1) [59,60]. The base plate and the weld attachments were clamped to the welding table during each welding step, as shown in Fig. 1. The specimen was held clamped following each welding sequence until it cooled down to 150 °C. According to [13], the sequence 1 to 4 is followed while placing the welds to limit misalignment and adhere to the temperature constraint when welding duplex.

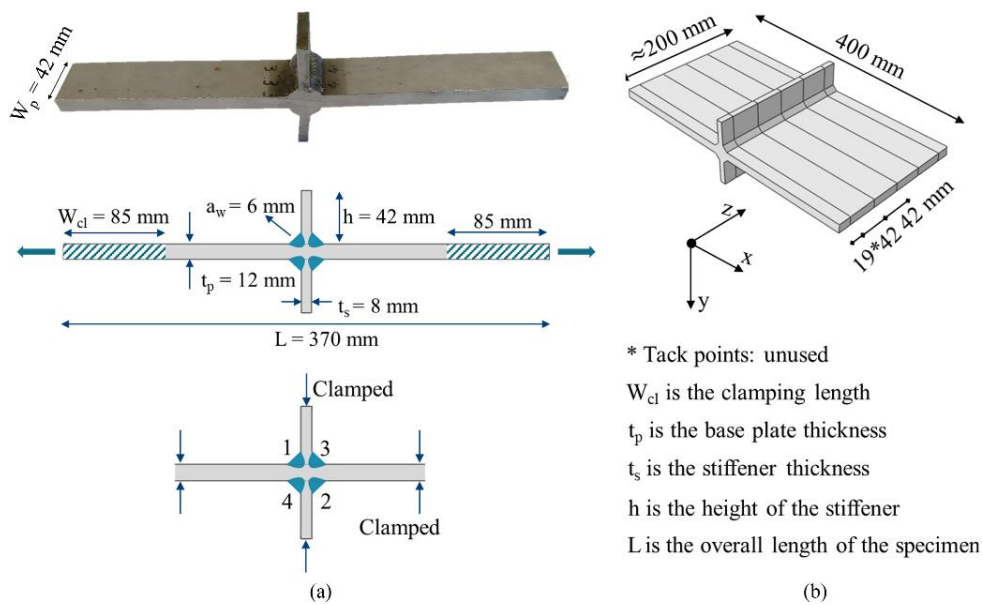


Fig. 1 Specimen preparation [41]: (a) geometry and welding sequence of the studied cruciform joint; (b) cutting scheme.

## 2.2.3 Fatigue strength modification

### 2.2.3.1 Geometrical misalignment factor – $k_m$

The IIW recommendations [51] take into account the secondary shell bending stresses and include the impact of misalignment on the HS stress (and subsequently fatigue strength). The proposed SN-curves by default permit a particular level of misalignment ( $k_m = 1.05$  for HSSM and 1.25 for NSM). The recommendation advises using  $k_m = 1.10$  for the examined stiffener using HSSM if the misalignment is not measured. The effective factor should be determined using Equations (1) – (3) if the



misalignment factor is to be assessed before fatigue testing. In the present study, the misalignment factor of the examined specimens was determined by DIC. Static images on either side of the specimen were taken, and the correlation between identical static images was created, giving the initial geometries. Fig. 2 illustrates a diagram of the observed geometry and additional explanations of the variables used in Equations (1) – (3).

$$k_{m,eff} = \frac{k_{m,calculated}}{k_{m,already\ covered}} \quad (1)$$

$$k_{m,calculated} = 1 + \frac{3y}{t} \cdot \frac{\tanh(\beta/2)}{\beta/2} \quad (2)$$

$$\beta = 1 + \frac{2l}{t} \sqrt{\frac{3\sigma_m}{E}} \quad (3)$$

where  $\sigma_m$  is the membrane stress (depending on the applied nominal stress range),  $t$  is the plate thickness,  $E$  is Young's modulus and  $2l$  is the length of the specimen.

As an example, according to Fig. 2,  $y$  is computed as 0.8mm,  $k_{m,calculated}$  is 1.15 and  $k_{m,already\ covered}$  is 1.05 in the IIW guidelines. The computed effective misalignment factor  $k_{m,eff}$  is thus obtained as 1.09, indicating that the specimen's HS stress ranges need to be raised by 9%. The specimens taken from each batch of the welded plates in Fig. 1 were discovered to have geometrical imperfections that were comparable to each other as well as IIW recommendations as further elaborated in [41]. This observation alongside the further investigations in [24,58] were the basis of applicability of hotspot stress method on the studied duplex welded components.

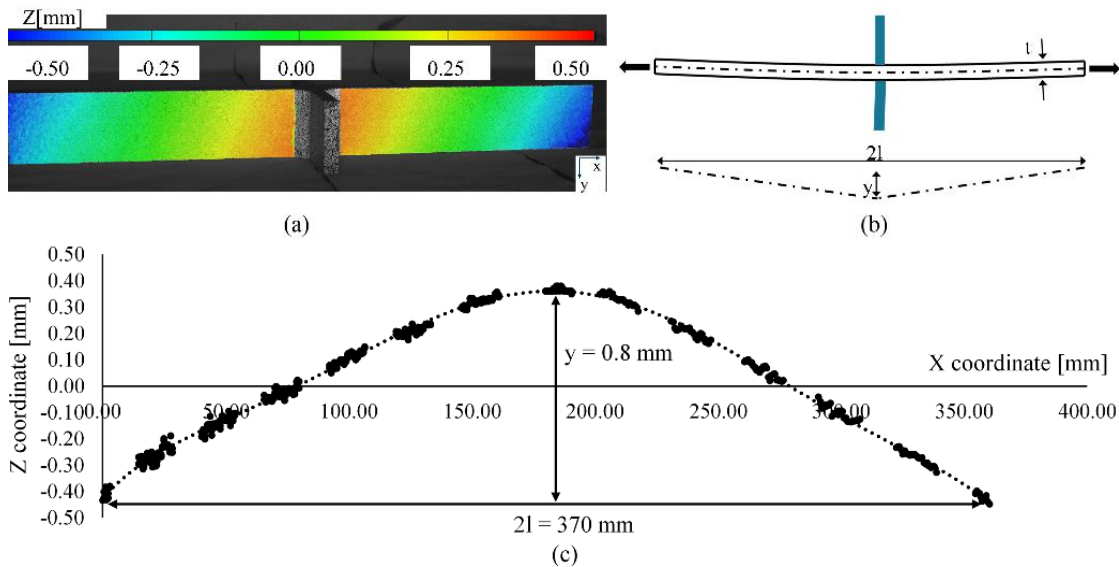


Fig. 2 Geometrical imperfections: (a) front view; (b) parameters for the formulation of  $k_m$ ; (c) calculation of the misalignment.



### 2.2.3.2 Modification with respect to stress ratio – $f(R)$

For particular stress ratios ( $R$ ), the IIW recommendation [51] suggests using a fatigue strength modification factor  $f(R)$ . This variable relies on how much residual stress is present in the examined component. According to [10,51], the fatigue resistance data (SN-curves) included in the Eurocode and IIW standards already account for high tensile residual stresses in the detail categories and are based on a wide range of experimental data collection. The following factors are included in the recommendation to distinguish between different residual stress levels: Low residual stress is present in seamless base plates and wrought products with residual stress less than  $0.2 f_y$ ; medium residual stress is present in small-scale, thin-walled structural elements with short welds; and high residual stress is present in two- or three-dimensional complex welded details with global residual stresses (thick-walled systems). No strength improvement is anticipated for stress ratios of  $R \geq 0$ . The stress ratio chosen for the test specimens in this paper is  $R = 0.3$ , and they fall into the category of medium to high residual stress. As a result, no strength enhancement was considered.

### 2.2.4 Fatigue test results of the welded specimens

#### 2.2.4.1 Fatigue resistance according to NSM

19 fatigue tests were carried out using an Instron 8802 series servo-hydraulic testing frame in order to attain the whole SN-curve of the studied detail. The fatigue resistance calculated in this chapter using the NSM is compared to the fatigue class FAT80 currently suggested in the IIW guidelines [51]. Secondly, the same is performed, except this time, the HSSM is used for the comparison. Based on a linear regression analysis with a fixed slope of  $m = 3$ , and a variable slope ( $m = m_{var}$ ) yielding the best fit against the experimental data (with lowest standard deviation and coefficient of variation), the fatigue resistance (i.e.,  $FAT_k$ , which is the stress range at  $2 \cdot 10^6$  cycles) is evaluated. The regression analysis is carried out in accordance with the IIW recommendations using Equations (4) to (6).

$$\log N = \log C - m \cdot \log \Delta \sigma \quad (4)$$

$$X_k = X_m \pm k \cdot Std v \quad (5)$$

$$k = 1.645 \left( 1 + \frac{1}{\sqrt{n}} \right) \quad (6)$$

where  $C$  is a constant that refers to the influence of construction detail in expression of fatigue strength [8],  $X_m$  is the mean of  $\log C$  values,  $X_k$  is the characteristic value related to  $X_m$ ,  $Stdv$  is the standard deviation of  $\log C$  values and  $k$  is a factor that depends on  $n$  which is the number of test samples.

The NSM is followed for constructing the SN-curves, where the characteristic fatigue strength ( $FAT_k$ ) is for a survival probability of 95% and the mean fatigue strength ( $FAT_m$ ) is for a survival probability of 50%. Table 3 and Fig. 3 provide an overview of the results and Fig. 4 depicts the typical failure mode and fracture surface analyses for one common test. When a fixed slope of  $m = 3$  is applied, it is reasonable to conclude that the NSM is applicable to the examined EN 1.4162 welded joints, with the lower bound being marginally above the codified detail category specified by the Eurocode and IIW guidelines [10,51]. However, it appears that using  $m_{var} = 4.00$  better agrees with the results of the experiment, offering the best match (see Fig. 5) with lower scatter in the data population as evidenced by the lower standard deviation and coefficient of variation in Table 3. However, the detail category and fatigue class in Eurocodes and IIW guidelines [10,51] are highly conservative in this instance. Similar findings can be seen in the literature [13–16,18–24,41] with respect to high strength metal grades. Interested readers can consult Section 5.1.1 of [41] for further explanation on the greater best-fitting slopes and resulting high conservatism. It is important to highlight that test results with a fatigue life  $N \geq 5 \cdot 10^6$  are excluded from the statistical analysis because, per [10,51], they exceed the constant amplitude fatigue limit (CAFL) in Eurocodes and are likely to fall into the ultra-high cycle fatigue range in IIW guidelines. It is also important to note that a two-sided confidence of 75% was employed while calculating the characteristic values. Further details related to the practical aspects of the test campaign (e.g., stress ranges and corresponding fatigue lives) can be found in [40].

Table 3 Fatigue strength characteristics of the welded EN 1.4162 specimen according to NSM.

SN-curve characteristics (95% fractile)	$FAT_k$ [N/mm <sup>2</sup> ]	$FAT_m$ [N/mm <sup>2</sup> ]	$Stdv$ [ $\sigma$ ]	Coefficient of variation (CoV)	Comparison with fatigue class FAT80
$m = 3.00$	83.99	110.78	0.174	0.014	+ 5
$m_{var} = 4.00$	111.77	124.07	0.088	0.006	+ 39.7%

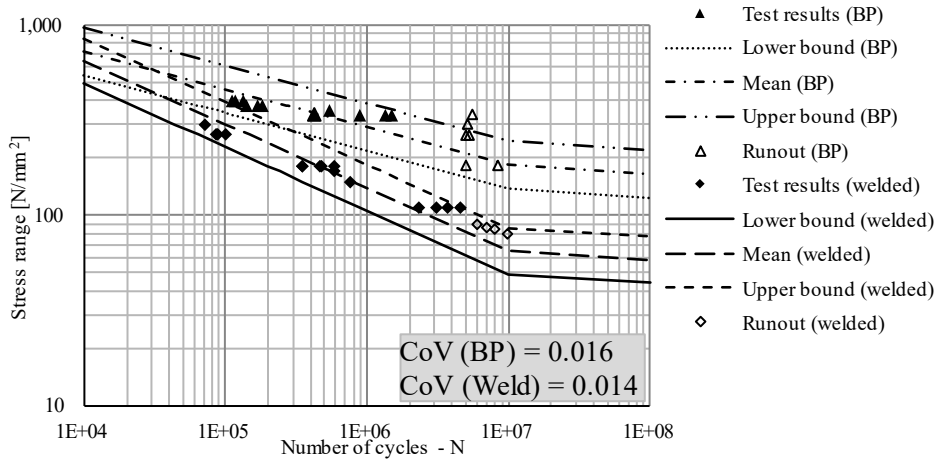


Fig. 3 SN-curves with fixed slope ( $m = 3$  for the welded specimens and  $m = 5$  for the base plates).

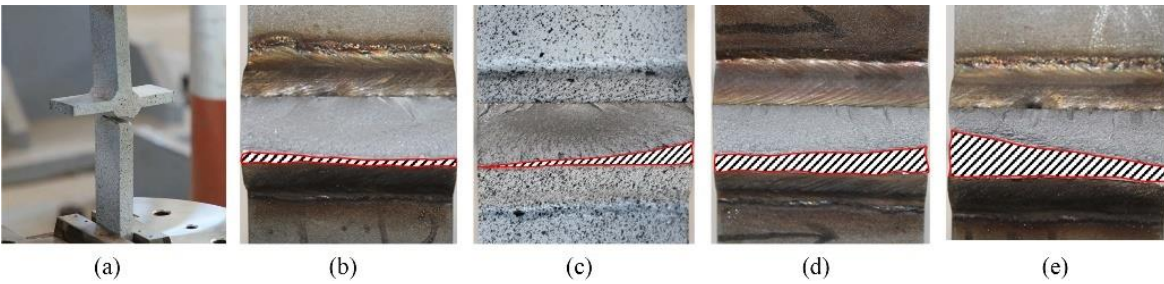


Fig. 4 Fatigue failure of the studied specimen (ductile fracture surface is hatched) [41][41]: (a) typical failure mode at the weld toe; (b) fracture surface at  $\Delta\sigma = 80 \text{ MPa}$ ; (c) fracture surface at  $\Delta\sigma = 110.4 \text{ MPa}$ ; (d) fracture surface at  $\Delta\sigma = 181.8 \text{ MPa}$ ; (e) fracture surface at  $\Delta\sigma = 264.7 \text{ MPa}$ .

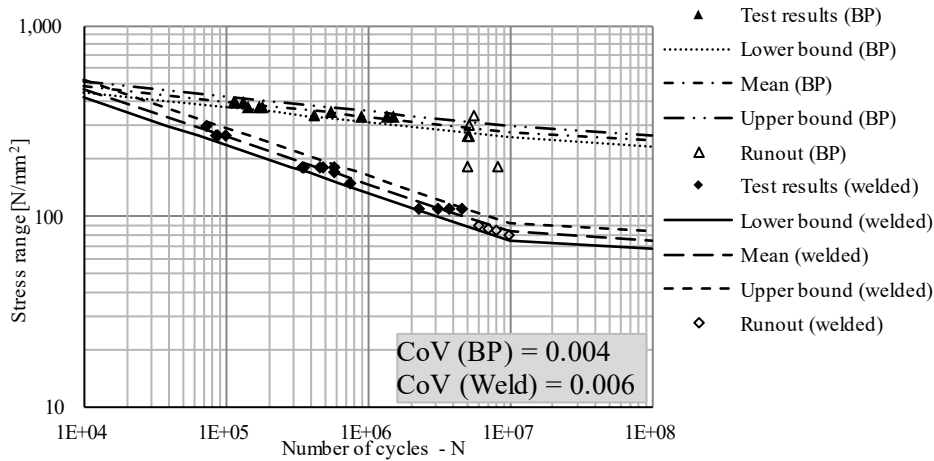


Fig. 5 SN-curves with variable slope ( $m_{var} = 4.00$  for the welded specimens and  $m_{var} = 12.43$  for the base plates).

### 2.2.4.2 Fatigue class according to HSSM

First, as described in Section 2.2.3, one cruciform sample from one batch was used to test the HS stress at various stress ranges while taking into account the detected misalignment factors. With a constant strain rate of  $0.00007 \text{ s}^{-1}$  according to [43], the same loading methodology as for the tensile testing on base plate coupons was applied. The cameras (Manta G-895 with 8.95 Megapixel resolution) were positioned 300 mm apart from the sample plane for the DIC measurements. As seen in Fig. 6 (b), the

speckle pattern was created by the airborne diffusion of black paint onto a uniformly painted white surface. The applied speckle pattern on the samples was no larger than 0.1 by 0.1 mm in size. The applied load is equivalent to a nominal stress range of the fatigue class, or 80 MPa, away from the weld toe. The measured strain field according to DIC and the sample with strain gauges can be seen in Fig. 6 for the applied stress state together with comparison of strain fields and HS stress for DIC vs. FEM.

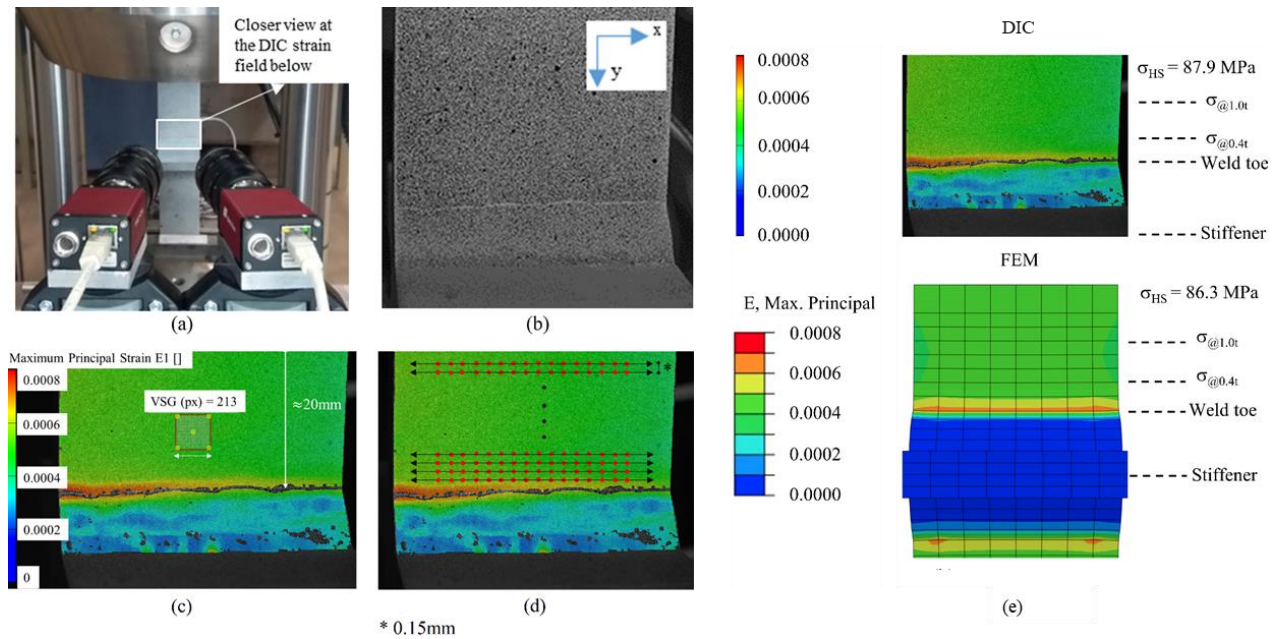


Fig. 6 Measurement of HS stress: (a) Test setup; (b) applied speckle pattern; (c) entire principal strain field; (d) procedure for extraction of principal strains; (e) comparison of strain fields and HS stress for DIC vs. FEM.

MatchID was used to process the measured DIC data. The parameters are chosen so that, without going beyond the recommended physical strain gauge size as per the IIW recommendation, the maximum principal stress component becomes insensitive to the virtual strain gauge (VSG) size. This is done so that a smooth principal stress pattern can be obtained without accuracy being lost owing to signal loss. Due to the relatively low level of elastic strains when the HS stress is measured, the signal to noise ratio may become a problem. This is typically prevented by choosing an optimal virtual strain gauge (VSG) size. A sensitivity analysis was carried out in order to choose the optimal parameters for post-processing of DIC data and further details are presented in Annex D of [40] and in [41].

As observed in Fig. 6 (d), the principal stress strips were measured in the x direction along the weld line in 0.15mm (6 pixels) increments along the vertical y axis, which essentially corresponds to the step size. The average of the principal stresses (and associated standard deviation) along each of

these strips was determined without including the half of the subset that is closest to the edge of the region of interest (ROI). This is done to prevent outliers brought on by image distortion close to the specimen boundaries. For the strain gauge (SG) measurements, Micro-Measurements® CEA-06-125UN-350 type SGs with 350 ohms grid resistance and 3.125 mm gauge length ( $0.2t < \text{gauge length} < 0.4t$ ) were employed. When HS stress is measured using strain gauges, a quasistatic loading is performed to match the appropriate stress range. In Fig. 7, where the average primary stress distribution was taken using the strategy shown in Fig. 6 (d), the results of the DIC and the SGs are compared.

Following the experimental studies, a finite element (FE) model was also created to serve as a simulated reference solution, with the parameters specified by the IIW guidelines [50,51,61]. Using C3D8R from the element library's hexahedral 8-noded linear solid elements with reduced integration, the FE analysis was carried out with Abaqus/Standard with an element size less than  $0.4 t$ . Mesh refinement was assigned until a distance of  $1.4 t$  from the weld toe (i.e., for the region where stress extrapolation is performed). Since linear elements are used, a minimum of 4 elements were used over the thickness in accordance with the guidelines [62]. The boundary conditions (BCs) in the reference model were selected so that the specimen is subjected to uniform tension, resulting in a nominal stress range in the flange that corresponds to the fatigue class of 80 MPa. Further details on the FEM of this detail can be found in the previously published article of the current paper's authors [41].

The average principal stress distribution was taken using the methods shown in Fig. 6 (d) for each of the five stress ranges applied during the fatigue test campaign ( $\Delta\sigma_1 - \Delta\sigma_5$ ), and a comparison of the measured and computed stress fields is shown in Fig. 7. The stress readout points using strain gauges is also marked in Fig. 7, and it demonstrates a great agreement with the stress results from DIC and FEM.

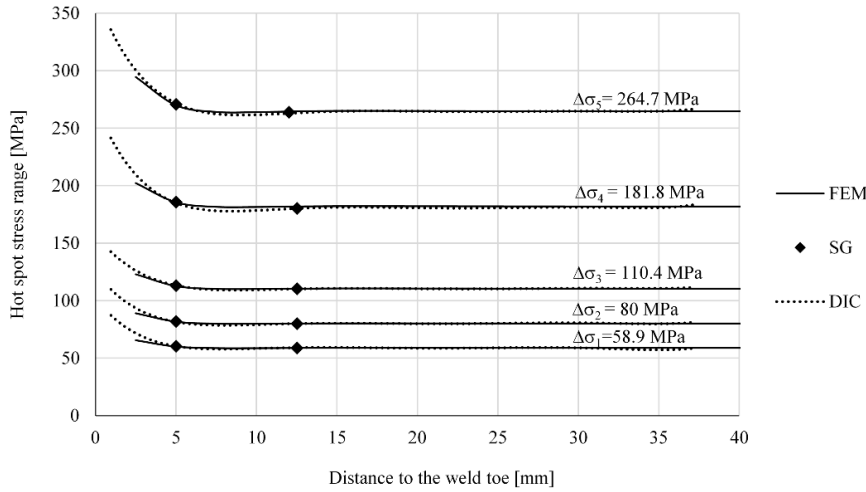


Fig. 7 Comparison of HS stress range according to DIC, SG and FEM [41].

Then, the test results were compared with the fatigue lives provided by the HSSM using the SCFs obtained from extrapolation of stresses in Fig. 7 in accordance with IIW recommendations [51] (see Fig. 8 and Table 4). The SN-curve characteristics assessed in relation to HS stress ranges are shown in Table 4 based on the linear regression analysis as outlined in Section 2.2.4. The lower bound of the HS stress range serves as the basis for the fatigue class, which is calculated as 102.95 MPa. The proposed reference detail in the IIW guideline is FAT100, which is in good agreement with the results. The lower bound calculated in Table 4 was obtained by taking into account both measured and computed SCFs (i.e., compiling DIC, SGs and FEM results). It is important to note that the measured misalignment factors ( $k_{m,eff}$ ) are included in the HS stress ranges. If IIW guideline's suggested  $k_m = 1.1$  for HS stress ranges is used, it results in a fatigue class of 100.55, which is very similar to the reference detail 100.

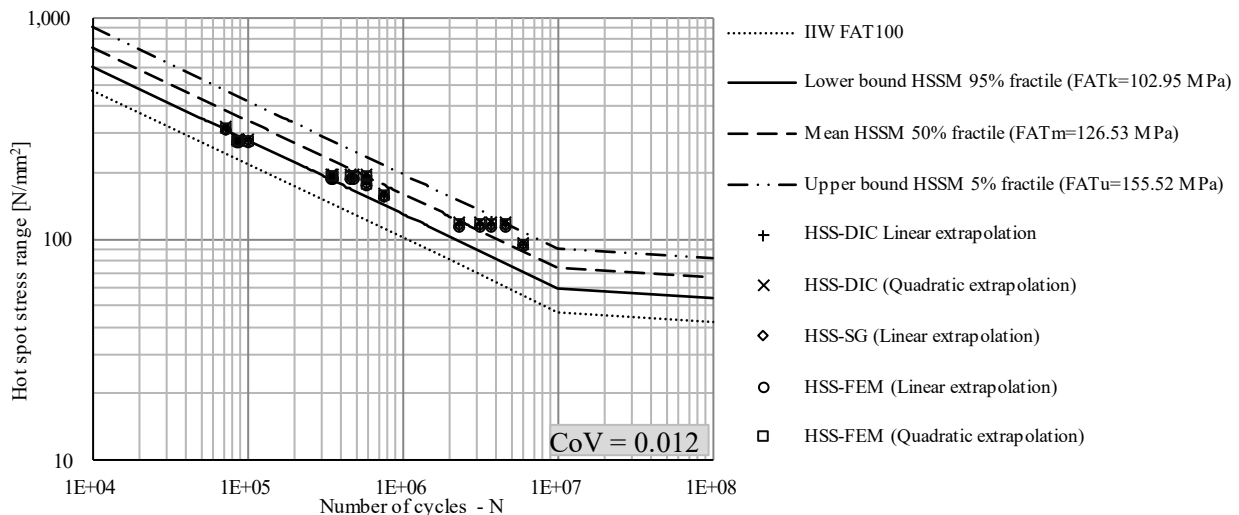


Fig. 8 SN-curve of the studied welded detail according to HS stress range including the misalignment effect.



Table 4 Fatigue strength characteristics of the welded EN 1.4162 specimen according to HSSM.

SN-curve characteristics (95% fractile)	$FAT_k$ (IIW) [N/mm <sup>2</sup> ]	$FAT_m$ (IIW) [N/mm <sup>2</sup> ]	$Stdv$ [ $\sigma$ ]	Coefficient of variation (CoV)	Comparison with fatigue class FAT100 (IIW) [51]
$m = 3$	102.95	126.53	0.146	0.012	+ 2.9%
$m_{var} = 3.77$	126.23	138.79	0.085	0.006	+ 26.2%

### 3 Applicability of current design provisions to high strength (stainless and carbon) metals

A larger database of fatigue test results was compiled to better emphasize how the present Eurocode standards apply to higher strength steels that are subjected to fatigue. Then, using finite element analyses, each database was again analysed at the nominal stress and hot spot stress ranges. Additionally, this was done to demonstrate that the hot spot stress method is applicable to materials other than duplex grades.

#### 3.1 Reassessment of the details

Transverse stiffeners, cope holes, and butt welds are the most representative details for bridges subjected to fatigue and are chosen for this section. The decision to choose these particular details was made in light of [57], which demonstrates that these three fatigue-prone elements are the most important ones in ordinary highway steel girder bridges. In this section, 313 transverse stiffener fatigue test results, 152 butt weld fatigue test results, and 55 cope hole fatigue test results from the literature were collated and re-evaluated in accordance with the NSM and HSSM. From Fig. 9 – Fig. 11, which together contain 22 references, one can see all the information that was included in the database. In this investigation, only details with nominal yield strengths  $f_y$  greater than 400 MPa have been taken into account. The nominal stress range for each reference data set has been converted to the HS stress range using SCFs derived from FEMs, with the model parameters selected using a sensitivity analysis as described in [40,58]. Based on the supplied (measured) data on geometrical and material properties from the matching reference, each test was simulated using the FEM. According to the IIW recommendations, no strength enhancement was anticipated for any reference data since the stress ratio  $R$  was larger than 0 and all data fell into the category of either medium or high residual stress [51]. According to [10], the size effect  $k_s$  was also taken into consideration for thicknesses greater than 25 mm.



1        Additionally, the geometrical misalignment factor discussed in Section 2.2.3, which increases  
2        the HS stress while taking into account secondary shell bending stresses, was observed. According to  
3        the IIW recommendations, an effective factor of 1.1 was employed if the reference source did not  
4        mention the misalignment, which increased the hot spot stress by 10%. For butt joints constructed in-  
5        shop in a flat position or for cruciform joints, the factor of 1.1 is acceptable. An estimated factor of  
6         $k_{m,eff} = 1.2$  is proposed for T-joints. However, as secondary shell bending stresses are not present  
7        when joints are loaded in pure bending, the misalignment factor should not be taken into account.  
8        Lower SCFs are anticipated since the bending fatigue setup naturally removes the secondary shell  
9        bending loads. This argument was covered and supported in [40]. Additionally, if it was measured and  
10       reported in the relevant reference, the weld topology (such as convexity, concavity, weld excess, etc.)  
11       is also included in the FEM.

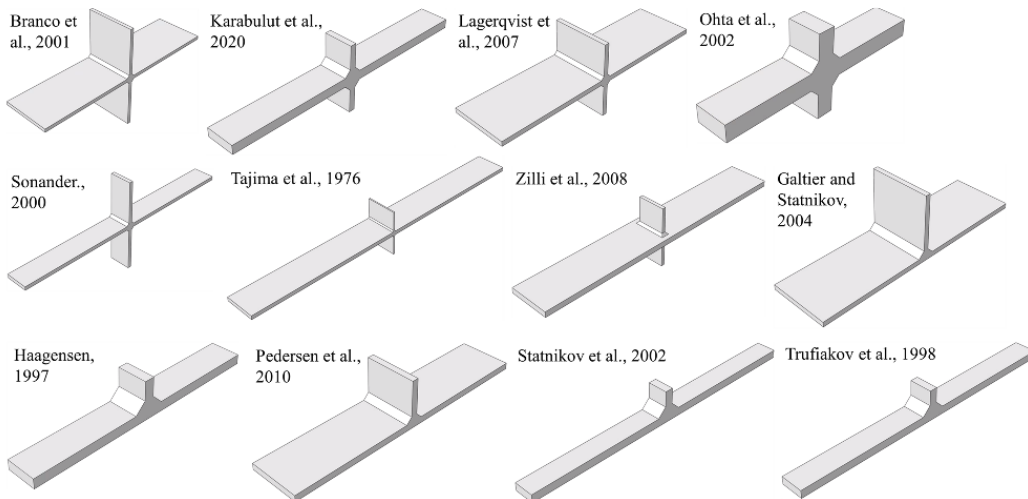


Fig. 9 Scheme of the transverse stiffeners in the re-evaluated database.

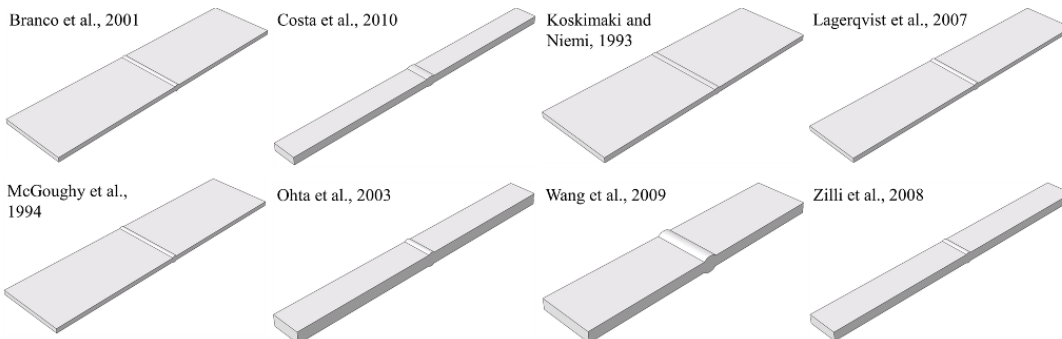


Fig. 10 Scheme of the butt welds in the re-evaluated database.

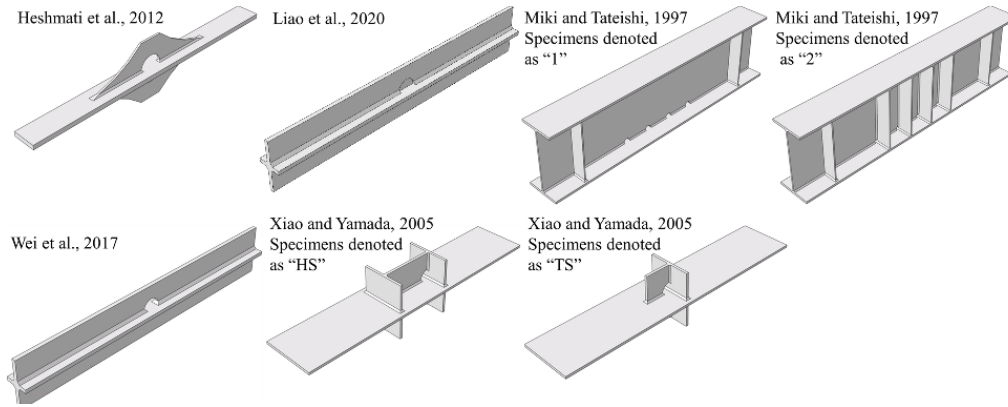


Fig. 11 Scheme of the cope holes in the re-evaluated database.

According to how fatigue tests were conducted – as advised in [63] – distinction between axial and bending loading was made for the computation of the SCF. A beam was modelled with boundary conditions (BCs) that do not impede Poisson's effects in the event of axial loading. A simply supported beam was modelled for bending, providing a four-point bending setup with no shear, and a constant bending moment in the centre, making it easier to calculate the nominal stress (and thus the SCF).

#### 3.1.1.1 Transverse stiffeners

The compiled literature data on the non load carrying fillet welds is shown in Table 5 according to the material grade, stress ratio  $R$ , joint type, plate thickness ( $t_p$ ), stiffener thickness ( $t_s$ ), welding procedures, and loading type. When the overall results are evaluated with the linear regression analysis, as shown in Table 6 and Fig. 12, the lower bound of the examined database results in a fatigue class  $FAT_{k,NSM} = 91.66$  MPa. Then, this value was compared with the 80 MPa recommended in [51] according to the NSM. One may therefore first deduce that the present codified fatigue class is approximately 15% conservative for transverse attachments composed of high strength carbon and duplex stainless steels, providing a possibility to upgrade the fatigue class  $FAT_k$  from 80 to 90 MPa. Table 6 and Fig. 13 show that the evaluated database's lower bound, as determined by the HSSM is  $FAT_{k,HSSM} = 103.43$  MPa, which is 3% higher than the reference fatigue class specified in the IIW standards (FAT100). The HSSM therefore offers better fatigue life prediction for the examined detail as also evidenced by slightly lower coefficient of variation in the data population.

1 Table 5 Characteristics of the collated database for non load-carrying fillet welds [58] ( $f_y \geq 400$  MPa).

Material	$R$	Joint type	$t_p$ [mm]	$t_s$ [mm]	Welding	Loading	Ref.
SS EN 1.4462	0.1/ 0.5	Cruciform	10	10	TIG	Axial	(Branco et al., 2001) [13]
HSS S700	0.1	T-joint	5	5	-	Bending	(Galtier and Statnikov, 2004) [14]
HSS S420	0.1	T-joint	20	20	SAW	Bending	(Haagensen, 1997) [16]
SS EN 1.4162	0.3	Cruciform	12	8	MAG	Axial	(Karabulut and Rossi, 2021a) [41]
HSS S700	0.2	Cruciform	8	8	MAG	Axial	(Lagerqvist et al., 2007) [18]
HSS S960	0.2	Cruciform	8	8	MAG	Axial	(Lagerqvist et al., 2007) [18]
HSS S1100	0.2	Cruciform	8	8	MAG	Axial	(Lagerqvist et al., 2007) [18]
HSS S570	0	Cruciform	20	20	MMA	Axial	(Ohta et al., 2002) [64]
HSS S700	0.1	T-joint	6	6	MAG	Bending	(Pedersen et al., 2010a) [20]
HSS S1100	0	Cruciform	8	8	MAG	Axial	(Sonander, 2000) [65]
HSS S420	0.1	T-joint	20	20	SAW	Bending	(Statnikov et al., 2002) [21]
HSLAS HT80	0	Cruciform	36	12	SAW	Axial	(Tajima et al., 1976) [22]
HSS S420	0.1	T-joint	20	20	-	Bending	(Trufiakov et al., 1998) [23]
SS EN 1.4462	0.1	Cruciform	20	12	SAW	Axial	(Zilli et al., 2008) [24]

2 Table 6 Fatigue strength of non load-carrying fillet welds according to NSM and HSSM ( $f_y \geq 400$  MPa).

Material	$n$	$FAT_{k,NSM}$ ( $m = 3$ ) [MPa]	Comparison with FAT80 [IIW]	$FAT_{k,HSSM}$ ( $m = 3$ ) [MPa]	Comparison with FAT100 MPa [IIW]	Ref.
SS EN 1.4462	14	134.89	+69%	146.13	+46%	(Branco et al., 2001) [13]
HSS S700	19	122.25	+53%	125.21	+25%	(Galtier and Statnikov, 2004) [14]
HSS S420	57	100.34	+25%	106.34	+6%	(Haagensen, 1997) [16]
SS EN 1.4162	19	83.99	+5%	101.02	+%1	(Karabulut and Rossi, 2021a) [41]
HSS S700	26	93.60	+17%	110.67	+11%	(Lagerqvist et al., 2007) [18]
HSS S960	30	102.83	+29%	121.57	+22%	(Lagerqvist et al., 2007) [18]
HSS S1100	14	118.47	+48%	140.07	+40%	(Lagerqvist et al., 2007) [18]
HSS S570	19	79.38	-1%	94.37	-6%	(Ohta et al., 2002) [64]
HSS S700	17	135.82	+70%	145.31	+45%	(Pedersen et al., 2010a) [20]
HSS S1100	47	74.54	-7%	84.99	-15%	(Sonander, 2000) [65]
HSS S420	9	95.83	+20%	100.98	+1%	(Statnikov et al., 2002) [21]
HSLAS HT80	11	90.89	+14%	106.09	+6%	(Tajima et al., 1976) [22]
HSS S420	14	99.93	+25%	105.71	+6%	(Trufiakov et al., 1998) [23]
SS EN 1.4462	17	88.18	+10%	101.04	+1%	(Zilli et al., 2008) [24]
Overall results	313	91.66 (CoV=0.024)	+15%	103.43 (CoV=0.023)	+3%	-

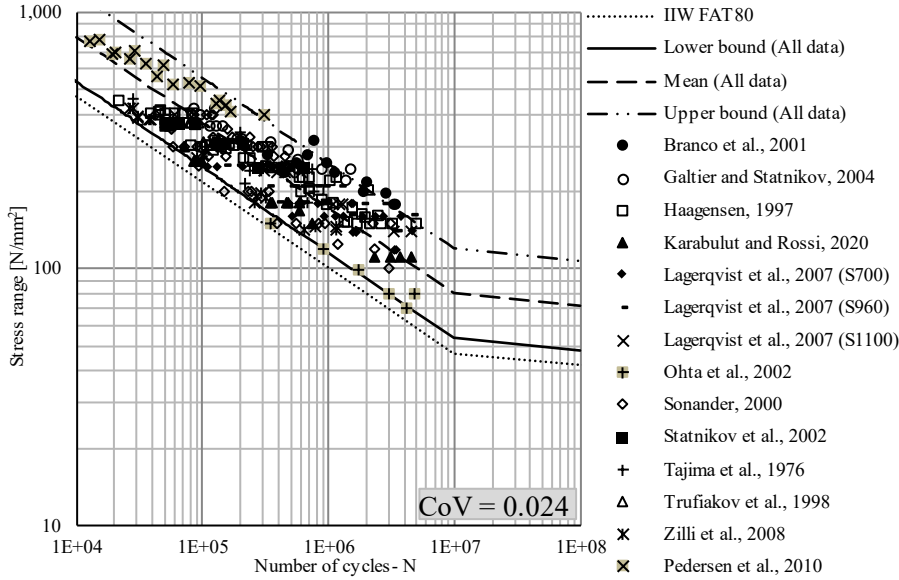


Fig. 12 SN-curves of non load-carrying fillet welds according to NSM ( $f_y \geq 400$  MPa).

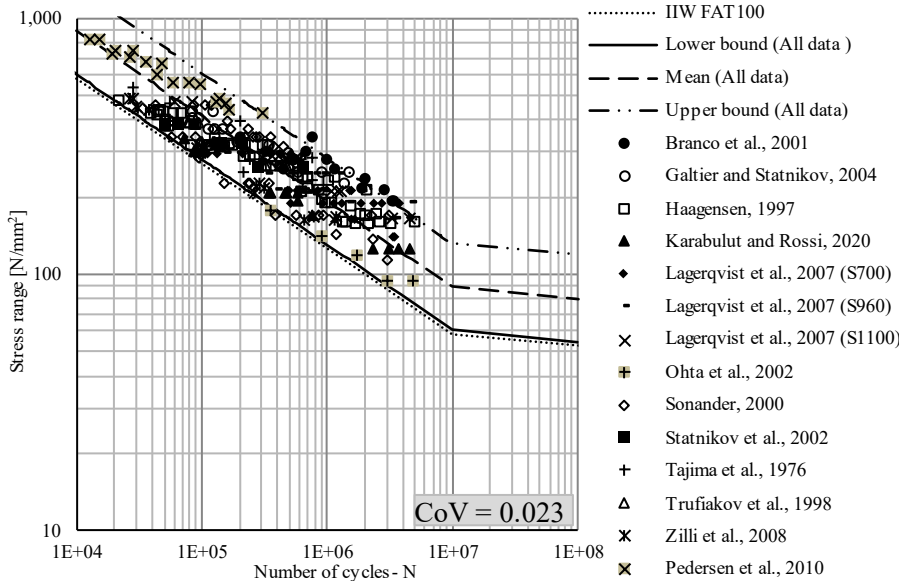


Fig. 13 SN-curves of non load-carrying fillet welds according to HSSM ( $f_y \geq 400$  MPa).

### 3.1.1.2 Butt welds

Table 7 lists the primary characteristics of the butt welds from the collected literature data. For welding, only X-bevel preparation is taken into account. Due to its ability to prevent geometrical misalignment on the flanges, this welding technique is the one used the most frequently in bridge applications. Once more, the database only contains materials with nominal yield strengths  $f_y \geq 400$  MPa. The excessive butt weld thickness,  $e_w$  (weld convexity), whose impact on HS stress was taken into account, affects the estimated SCF. If the bevel angle  $\theta$  is not specified, it is assumed to be  $60^\circ$  in the FEM of the detail that complies with quality level B in [53]. Table 8 and Fig. 14 provide an overview of the NSM results, and it can be seen that the lower bound of the evaluated database for butt welds  $FAT_{k,NSM} =$

92.86 MPa is higher than the recommended one of 80 MPa, once again providing a chance to upgrade the fatigue class  $FAT_{k,NSM}$  from 80 to 90 MPa. The HSSM again produces more representative results, as shown in Table 8 and Fig. 15, with only a 5-percent difference when the complete database is included (the lower bound is  $FAT_{k,HSSM} = 105.10$  MPa compared to FAT100 according to IIW recommendation).

Table 7 Characteristics of the collated database for load-carrying butt welds [58] ( $f_y \geq 400$  MPa).

Material	$R$	$t_p$ [mm]	$\theta$ [°]	Welding	Loading	Ref.
SS EN 1.4462	0.1/0.5	10	90	TIG	Axial	(Branco et al., 2001) [13]
HSS DOMEX 600 DC	0	5	90	MAG	Axial	(Costa et al., 2010) [66]
SS Polarit 803	0.1	10	60	MAG	Axial	(Koskimaki and Niemi, 1993) [67]
HSS S700/S960	0.2	8	100	MAG	Axial	(Lagerqvist et al., 2007) [18]
SS EN 1.4462	0.1	10	90		Axial	(McGoughy, 1994) [68]
CS SPV490	0/0.5	20	60	SAW	Axial	(Ohta et al., 2002) [64]
HSS SS800	0.05/0.1	8			Axial	(Wang et al., 2009) [69]
SS EN 1.4462	0.1	30	60	SAW	Axial	(Zilli et al., 2008) [24]

Table 8 Fatigue strength of load-carrying butt welds according to NSM and HSSM ( $f_y \geq 400$  MPa).

Material	$n$	$FAT_{k,NSM}$ ( $m = 3$ ) [MPa]	Comparison with FAT80 [IIW]	$FAT_{k,HSSM}$ ( $m = 3$ ) [MPa]	Comparison with FAT100 MPa [IIW]	Ref.
SS EN 1.4462	13	131.38	+64%	137.06	+37%	(Branco et al., 2001) [13]
HSS DOMEX 600 DC	18	110.34	+38%	124.43	+24%	(Costa et al., 2010) [66]
SS Polarit 803	10	113.61	+42%	128.61	+29%	(Koskimaki and Niemi, 1993) [67]
HSS S700/S960	42	96.78	+21%	111.07	+11%	(Lagerqvist et al., 2007) [18]
SS EN 1.4462	8	113.55	+42%	130.30	+30%	(McGoughy, 1994) [68]
CS SPV490	26	89.01	+11%	100.04	+0.04%	(Ohta et al., 2002) [64]
HSS SS800	21	93.77	+17%	106.91	+7%	(Wang et al., 2009) [69]
SS EN 1.4462	14	80.23	+0.3%	90.15	-10%	(Zilli et al., 2008) [24]
Overall results	152	92.86 (CoV=0.029)	+16%	105.10 (CoV=0.028)	+5%	

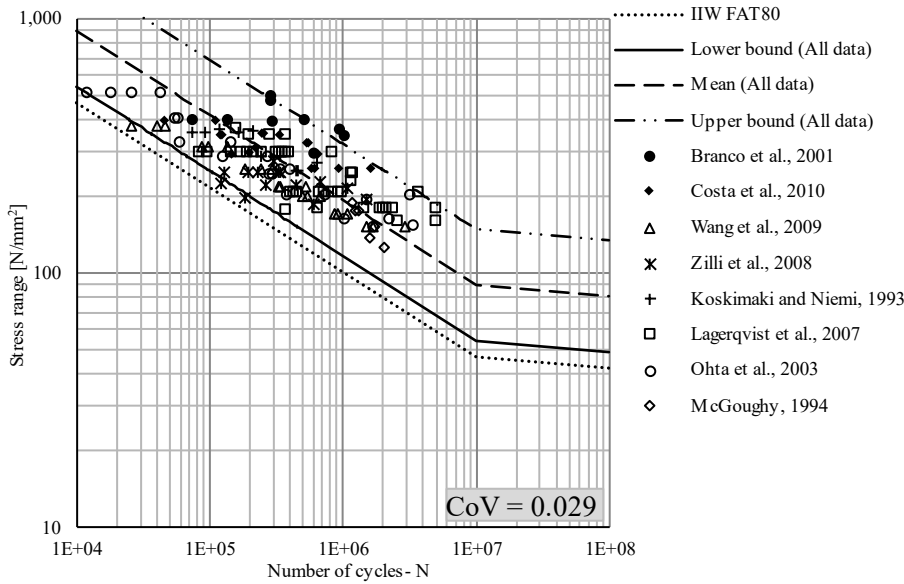


Fig. 14 SN-curves of load-carrying butt welds according to NSM ( $f_y \geq 400$  MPa).

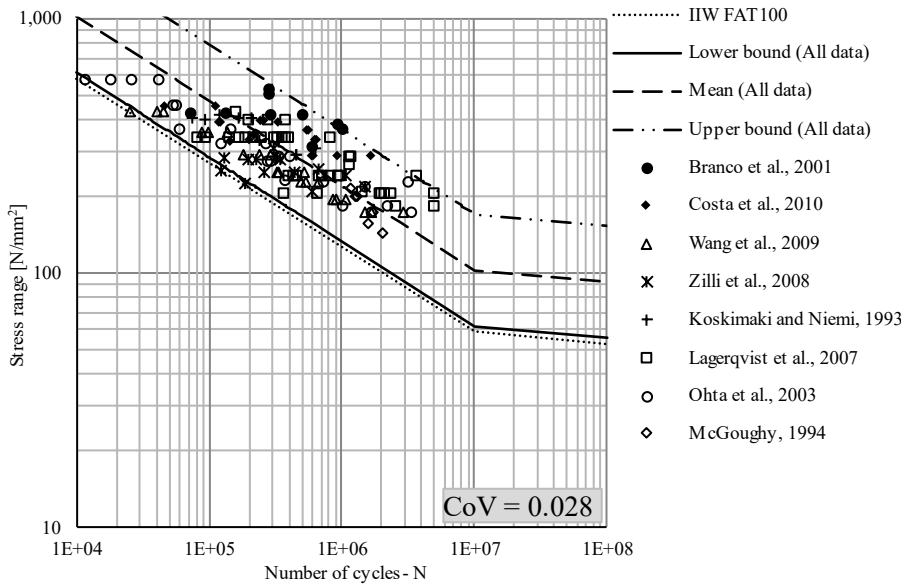


Fig. 15 SN-curves of load-carrying butt welds according to HSSM ( $f_y \geq 400$  MPa).

### 3.1.1.3 Cope holes

Table 9 displays the literature database of the cope holes that has been compiled. In the literature, there is little experimental study on cope holes. Unfortunately, there was no research on high strength steel grades with  $f_y \geq 400$  MPa. As a result, the highest strength classes were taken into consideration in this case, with a yield strength  $f_y \geq 345$  MPa. The characteristic fatigue strength for the test results of [70] in Table 10 is significantly lower than the fatigue class of 71 MPa according to [51]. The reason for this is that the authors used a 3-point bending configuration and it involved a combination of shear and normal stresses on the area surrounding the cope hole. The presence of shear stress at the possible crack initiation point of the cope hole is detrimental to the fatigue resistance (the ratio of  $\tau/\sigma$ ),

as stated in the original work and later references [70–74]. Therefore, the results of [70] were not included in the statistical analysis for consistency, ensuring that the assessment adheres to the same fatigue class without being influenced by shear stresses. The lower bound of the evaluated database for the cope holes results in a fatigue class of  $FAT_{k,NSM} = 54.38$  MPa, which is 23% lower than the one specified in the code, as shown in Table 10 and Fig. 16. The NSM results in unsafe prediction of the fatigue resistance for the cope holes constructed of steel grades with  $f_y \geq 345$  MPa, in contrast to non load-carrying fillet welds and butt welds. The HS stress ranges for each analysed detail here are much larger than the nominal ones since the SCFs for cope holes are significantly higher than those for transverse stiffeners and butt welds because quadratic extrapolation is advised for cope holes. As a result, as shown in Fig. 17, the HSSM once again provides a more representative assessment of the fatigue resistance for cope holes made of the investigated high-strength grades, as also evidenced by much lower coefficient of variation among the evaluated data population.

Table 9 Characteristics of the collated database for cope holes [58] ( $f_y \geq 345$  MPa).

Material	$R$	$t_p$ [mm]	$t_w$ [mm]	$\tau/\sigma$	Radius [mm]	Welding	Loading	Ref.
S355	0.1	20	8	0	50		Axial	(Heshmati, 2012) [72]
Q345C	0.1	16	16	0	40		Axial	(Liao et al., 2020) [75]
Q345C	0.1	16	16	0	40		Axial	(Wei et al., 2017) [74]
SM490YA	0.16- 0.25	9	9	0	35	MAG	Axial	(Xiao and Yamada, 2005) [76]
SM490YA		5	5	0.7-1	25-50		Bending	(Miki and Tateishi, 1997) [70]

Table 10 Fatigue strength of cope holes according to NSM and HSSM ( $f_y \geq 345$  MPa).

Material	$n$	$FAT_{k,NSM}$ ( $m = 3$ ) [MPa]	Comparison with FAT71 [IIW]	$FAT_{k,HSSM}$ ( $m = 3$ ) [MPa]	Comparison with FAT100 MPa [IIW]	Ref.
S355	4	86.78	+22	103.35	+3%	(Heshmati, 2012) [72]
Q345C	3	60.36	-15%	108.24	+8%	(Liao et al., 2020) [75]
Q345C	9	56.75	-20%	107.60	+8%	(Wei et al., 2017) [74]
SM490YA	17	76.51	+8%	107.48	+7%	(Xiao and Yamada, 2005) [76]
SM490YA	22	19.63	-72%	35.21	-65%	(Miki and Tateishi, 1997) [70]
Overall results	55	54.38 (CoV=0.019)	-23%	104.79 (CoV=0.006)	+5%	



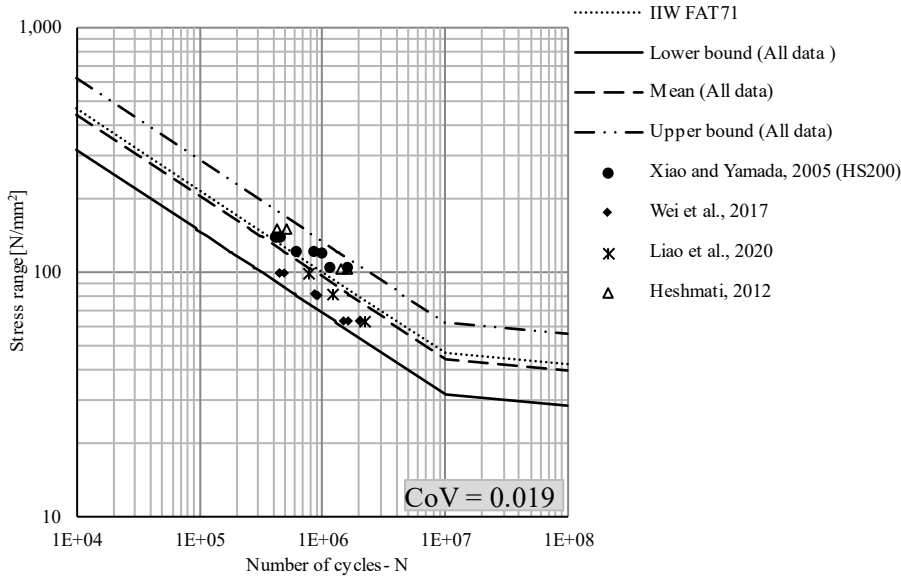


Fig. 16 SN-curves of cope holes according to NSM ( $f_y \geq 345$  MPa).

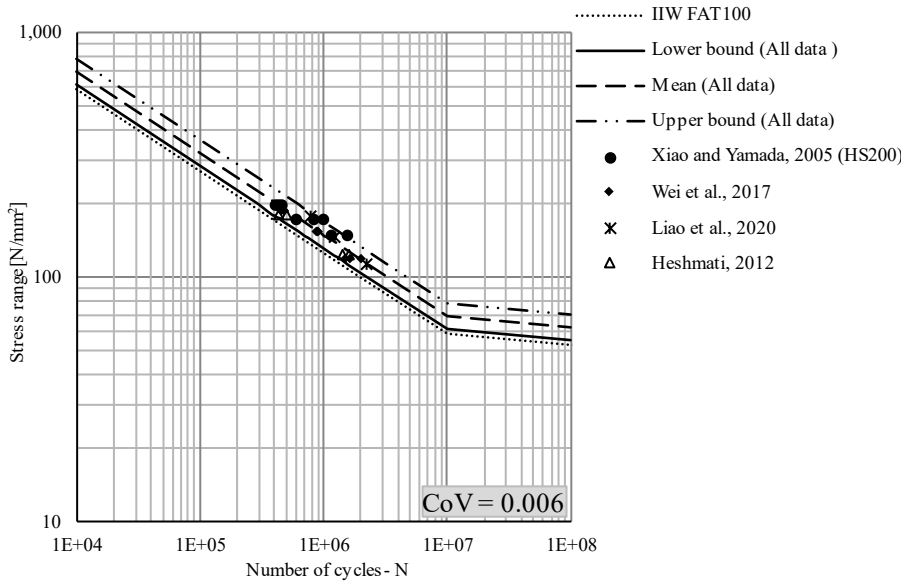


Fig. 17 SN-curves of cope holes according to HSSM ( $f_y \geq 345$  MPa).

## 4 Reliability Assessment

### 4.1 Two-parameter Weibull distribution

Weibull models are frequently employed in survival analysis and reliability studies. This chapter evaluated the SN-curves proposed in Section 3 using the conventional two-parameter Weibull distribution. Equation (7) provides the cumulative probability function with two parameters [77] while equation (8) based on Bernard's median rank [78] provides the likelihood of failure at a specific time:

$$P(N) = 1 - e^{-\left[\frac{N}{\alpha_w}\right]^{\beta_w}} \quad (7)$$

$$P(N_i) = \frac{i-0.3}{n+0.4} \quad (8)$$

1 where  $N$  is the number of cycles at failure,  $\alpha_w$  is the scale parameter and  $\beta_w$  is shape parameter,  $N_i$  is  
 2 the number of cycles at a given order,  $i$  is the order number of failures and  $n$  is the sample size.

3 Four distinct techniques were used to estimate the scale and shape parameters  $\alpha_w$  and  $\beta_w$ ,  
 4 following the strategy suggested in [79]: Equation (9) describes the Maximum Likelihood Method  
 5 (MLM) [79], equations (10) – (13) describe the Method of Moments (MM) [80], equations (14) and  
 6 (15) describe the Linear Least Squares Method (LLSM) [81], equations (16) and (17) describe the  
 7 Weighted Linear Least Squares Method (WLLSM) [82].

$$L(\alpha_w, \beta_w | N) = \left( \frac{\beta_w}{\alpha_w \beta_w} \right)^n \prod_{i=1}^n \left\{ N_i [\beta_w - 1] \exp \left[ - \left( \frac{\sum N_i}{\alpha_w} \right)^{\beta_w} \right] \right\} \quad (9)$$

$$\mu_k = \frac{1}{n} \sum_{i=0}^n N_i^k \quad (10)$$

$$M_1 = \alpha_w \Gamma \left( 1 + \frac{1}{\beta_w} \right) \quad (11)$$

$$M_2 = \alpha_w^2 \Gamma \left( 1 + \frac{2}{\beta_w} \right) \quad (12)$$

$$\frac{\mu_2}{\mu_1^2} = \frac{\Gamma \left( 1 + \frac{2}{\beta_w} \right)}{\Gamma^2 \left( 1 + \frac{1}{\beta_w} \right)} \quad (13)$$

$$\alpha_w = \frac{n \sum_{i=1}^n X_i Y_i - \sum_{i=1}^n X_i \sum_{i=1}^n Y_i}{n \sum_{i=1}^n X_i^2 - \left( \sum_{i=1}^n X_i \right)^2} \quad (14)$$

$$\beta_w = \exp \left( \frac{\sum_{i=1}^n Y_i - \alpha_w \sum_{i=1}^n X_i}{n \alpha_w} \right) \quad (15)$$

$$\alpha_w = \frac{\sum_{i=1}^n w_i \sum_{i=1}^n w_i X_i Y_i - \sum_{i=1}^n w_i X_i \sum_{i=1}^n w_i Y_i}{\sum_{i=1}^n w_i \sum_{i=1}^n w_i X_i^2 - \left( \sum_{i=1}^n w_i X_i \right)^2} \quad (16)$$

$$\beta_w = \exp \left( \frac{\sum_{i=1}^n w_i Y_i - \alpha_w \sum_{i=1}^n w_i X_i}{\alpha_w \sum_{i=1}^n w_i} \right) \quad (17)$$

8 where  $L$  is the likelihood function of the Weibull distribution,  $n$  is the sample size,  $\mu_k$  are the sampling  
 9 moments,  $M_1$  and  $M_2$  are the first two population moments,  $\Gamma$  is the mathematical gamma operator,  $X_i$   
 10 and  $Y_i$  are the two linear parameters dependent on  $N_i$  (more details in [83]) and  $w_i$  is the approximation  
 11 of weights which depends on the estimated values of the accumulated probability function  $P(N_i)$ .

12 In the case of MLM, the log-likelihood function is used to estimate the Weibull parameters.  
 13 They are calculated by using interactive numerical methods to maximize the logarithmic function. In  
 14 the case of MM,  $N$  is specified as an independent variable with an identical distribution, making it easy  
 15 to estimate the Weibull distribution parameters by approximating the solution with two population  
 16 moments ( $M_1$  and  $M_2$ ). Equation (13), which represents the sample's coefficient of variation, is only

1   reliant on the shape parameter  $\beta_w$ , and can be obtained by relating equations (12) – (14), using  
2   mathematical operations. The final solution is obtained by Newton-Raphson method. In the case of  
3   LLSM, to create a linear model for the  $X_i$  and  $Y_i$  parameters as a function of  $N_i$ , the first step is to take  
4   the logarithm of equation (7). Then, as explained in [81], a linear regression is used to obtain the  
5   estimation of the Weibull parameters. Additionally, in case of WLLSM, a separate level of importance  
6   is assigned to each data set element, as described in [82]. According to goodness-of-fit statistics, four  
7   distinct Weibull distribution functions were produced by the four estimations for  $\alpha_w$  and  $\beta_w$ . As a  
8   result, the Weibull distribution's agreement with the experimental fatigue data was assessed using three  
9   distinct tests: (i) equation (18) giving the Kolmogorov-Smirnov (KS) test; (ii) equation (19)  
10   representing the Anderson-Darling (AD) test; and (iii) equation (20) performing the  $\chi^2$  test. Finally,  
11   using the four alternative Weibull distribution functions, the fatigue resistances are calculated for three  
12   different reliability levels (RL): 90, 95, and 97.5%.

$$KS = \sup |P(N_i) - P(N_i)_{est.method}| \quad (18)$$

$$AD = -n - \frac{1}{n} \sum_{i=1}^n \{(2i - 1)(\log (P(N_i)_{est.method}) + \log (1 - P(N_{n+1-i})_{est.method}))\} \quad (19)$$

$$\chi^2 = \frac{(P(N_i)_{est.method} - P(N_i))^2}{P(N_i)} \quad (20)$$

#### 13   **4.2   Estimation of scale parameter $\alpha_w$ and shape parameter $\beta_w$**

14   The test results in Chapter 3.1 were analysed according to the two-parameter Weibull distribution  
15   function for reliability and survival analysis. Fig. 18 – Fig. 20 show the correlation graphs between the  
16   cumulative survival probability and the normalized number of cycles derived using the Weibull  
17   distributions (via four different estimating methods) and a normal distribution. In Fig. 18 – Fig. 20, the  
18   analyses are repeated twice both at the nominal stress (NSM) range and hot spot stress (HSSM) range  
19   as elaborated in Chapter 3.1. The estimations of Weibull distribution parameters  $\alpha_w$ ,  $\beta_w$ , and  
20   respective detail categories are presented in Table 11 – Table 13.

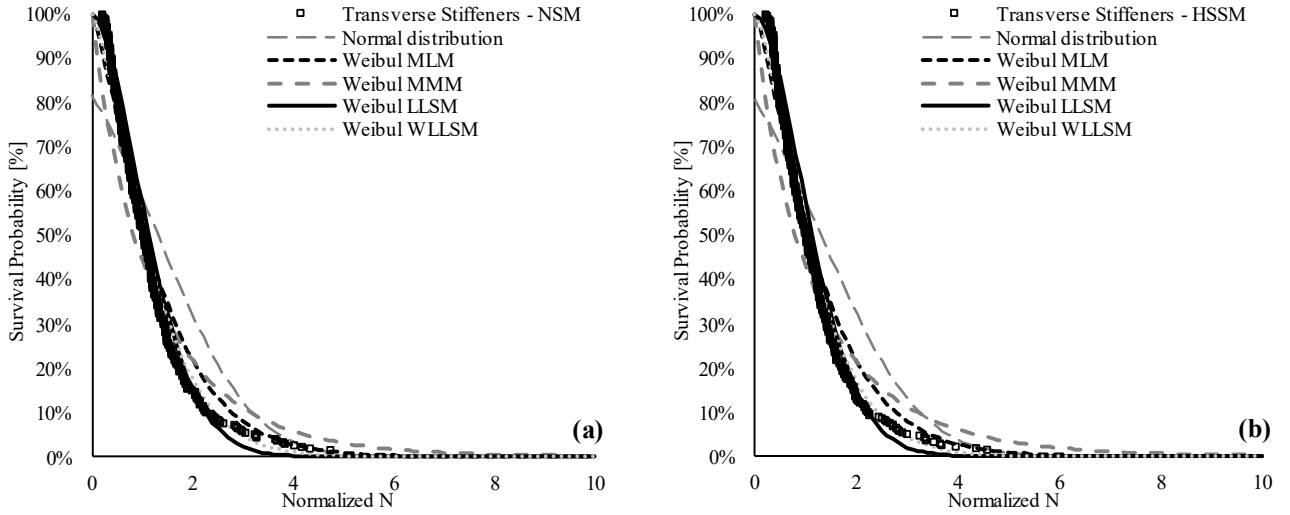


Fig. 18 Weibull distribution charts of the collated transverse stiffeners in Section 3.1: (a) acc. to NSM; (b) acc. to HSSM.

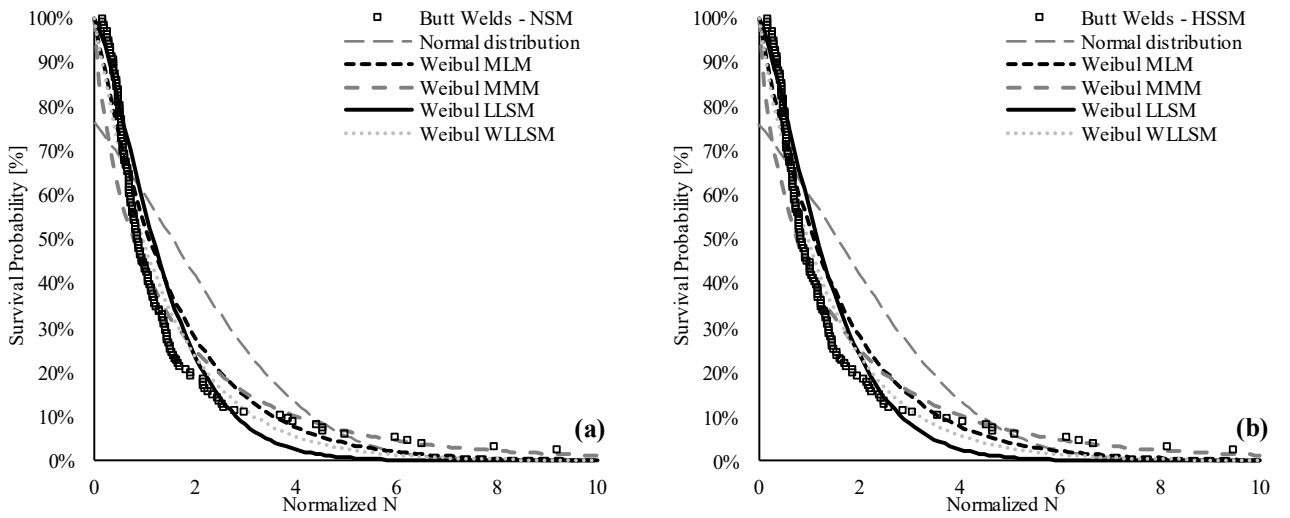


Fig. 19 Weibull distribution charts of the collated butt welds in Section 3.1: (a) acc. to NSM; (b) acc. to HSSM.

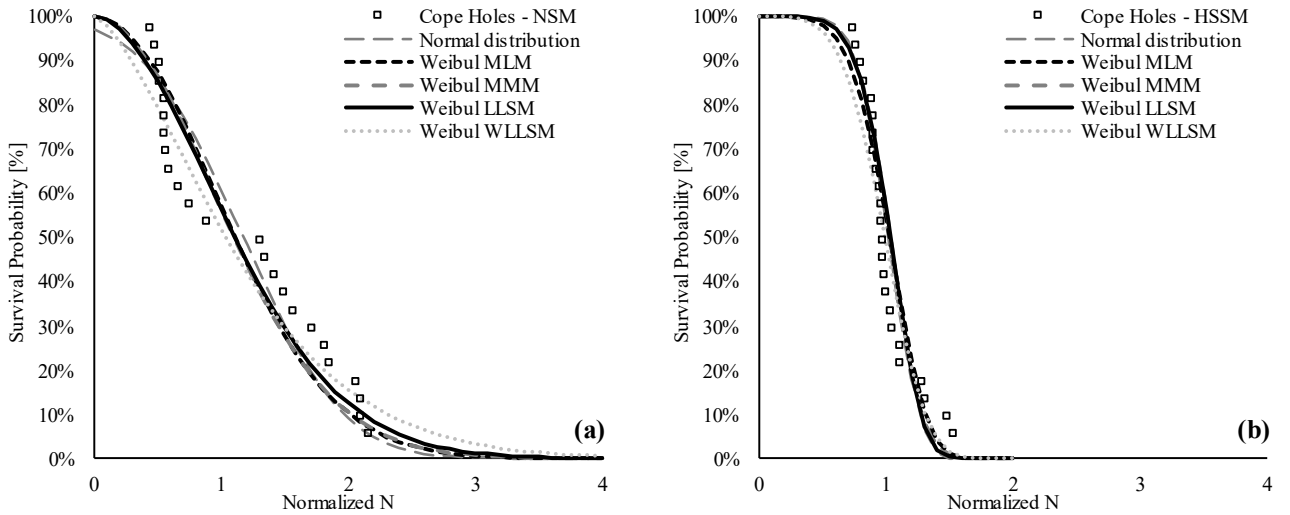


Fig. 20 Weibull distribution charts of the collated cope holes in Chapter 3.1: (a) acc. to NSM; (b) acc. to HSSM.

Table 11 Estimation of Weibull parameters, goodness-of-fit and fatigue strength for the collated transverse stiffeners in Chapter 3.1.

		Method – Nominal Stress				Method – Hotspot stress			
		MLM	MMM	LLSM	WLLSM	MLM	MMM	LLSM	WLLSM
$\alpha_w$		1.25	0.90	1.73	1.39	1.24	0.86	1.77	1.40
$\beta_w$		1.42	1.24	1.39	1.34	1.41	1.21	1.38	1.32
Goodness-of-fit	<i>KS</i>	0.11	0.22	0.07	0.10	0.13	0.26	0.07	0.11
	<i>AD</i>	7.12	22.55	2.27	4.27	8.36	27.24	2.49	5.12
	$\chi^2$	14.55	65.83	3.03	10.12	19.47	88.17	4.06	13.47
Fatigue strength [MPa]	RL 97.5 %	57.68	37.69	75.34	62.40	63.74	39.23	84.97	69.79
	RL 95 %	69.65	48.97	86.30	73.93	77.07	51.54	97.08	82.58
	RL 90 %	84.41	63.93	99.11	87.87	93.54	68.08	111.22	98.04

Table 12 Estimation of Weibull parameters, goodness of fit and fatigue strength for the collated butt welds in Chapter 3.1.

		Method – Nominal Stress				Method – Hotspot stress			
		MLM	MMM	LLSM	WLLSM	MLM	MMM	LLSM	WLLSM
$\alpha_w$		1.02	0.73	1.36	1.01	1.01	0.72	1.34	1.00
$\beta_w$		1.57	1.28	1.52	1.39	1.58	1.27	1.53	1.39
Goodness-of-fit	<i>KS</i>	0.13	0.25	0.14	0.15	0.14	0.25	0.14	0.15
	<i>AD</i>	6.14	12.88	6.64	5.83	6.15	13.07	6.62	5.83
	$\chi^2$	8.70	35.80	3.21	11.40	8.64	36.22	3.17	11.28
Fatigue strength [MPa]	RL 97.5 %	53.55	31.18	71.70	50.97	60.25	34.61	80.95	57.37
	RL 95 %	67.50	43.04	85.29	64.35	76.14	47.98	96.45	72.60
	RL 90 %	85.47	59.78	101.79	81.63	96.64	66.96	115.33	92.30

Table 13 Estimation of Weibull parameters, goodness of fit and fatigue strength for the collated cope holes in Chapter 3.1.

		Method – Nominal Stress				Method – Hotspot stress			
		MLM	MMM	LLSM	WLLSM	MLM	MMM	LLSM	WLLSM
$\alpha_w$		2.02	1.96	1.85	1.50	4.91	5.90	5.79	4.29
$\beta_w$		1.33	1.32	1.35	1.32	1.10	1.10	1.10	1.08
Goodness-of-fit	<i>KS</i>	0.18	0.17	0.16	0.15	0.18	0.20	0.20	0.17
	<i>AD</i>	2.02	1.96	1.85	1.50	1.43	1.70	1.66	1.50
	$\chi^2$	0.73	0.74	0.74	1.29	0.95	0.61	0.64	1.81
Fatigue strength [MPa]	RL 97.5 %	45.07	44.13	42.77	36.36	95.44	44.13	99.02	91.28
	RL 95 %	50.64	49.77	48.58	42.55	100.12	49.77	103.12	96.43
	RL 90 %	57.02	56.25	55.32	49.95	105.14	56.25	107.49	101.98

### 4.3 Discussion of reliability assessment results

One of the first interpretations from Table 11 to Table 13 is that the  $\beta_w$  – shape parameter is always greater than 1.0, which gives confidence in that all samples were suffering from fatigue failure without

experiencing premature failure or other forms of failure. This is evidenced by the bathtub curve where  $\beta_w > 1$  refers to failure due to wear-out (e.g., fatigue) as shown in Fig. 21 [84].

As can also be seen in Table 11– Table 13, linear least squares method (LLSM) leads to a better fitting and more accurate results using a Weibull distribution, for all the studied data population. This is evident in Fig. 18 – Fig. 20 where a better graphical fit is obtained as well as in Table 11 – Table 13 where the lowest  $\chi^2$  test results are consistently attained. The proposals to upgrade the fatigue class –  $FAT_k$  from 80 to 90 MPa for transverse stiffeners and butt welds are proven valid as the reliability levels using a Weibull distribution is higher than 0.90. This is supported by the obtained fatigue strength –  $FAT_k = 99.11$  MPa for transverse stiffeners and 101.79 MPa for butt welds with  $RL = 90\%$ , while 86.30 MPa and 85.29 MPa respectively are obtained for  $RL = 95\%$ . It must be noted that 0.90 reliability is acceptable for engineering applications to propose normative upgrades [85]. Similar reliability level is achieved (with  $RL = 90\%$ ) – this time for all details – when the evaluation is made according to the hotspot stress method.

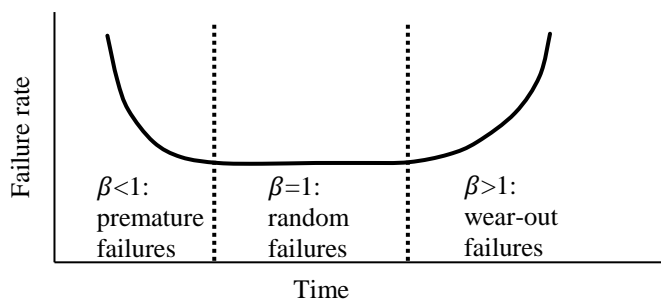


Fig. 21 Bathtub curve failure modes.

## 5 Conclusions

This paper first presents the findings of an experimental campaign examining the fatigue behavior of welded cruciform joints and unwelded base plates fabricated from high-strength duplex EN 1.4162 grade. The nominal stress method and the hot spot stress method are used to evaluate the test results. The fatigue strength curves (SN-curve) with a standardized fixed slope of  $m$  equal to 3.0 leads to the conclusion that the proposed Eurocode and IIW formulae are slightly conservative when the nominal stress technique is considered. The experimental results are thought to be better represented by a higher slope coefficient  $m$  (i.e., a flatter SN-curve).

1 However, in that case, the detail category or fatigue class becomes too conservative. Conversely, the  
2 hot spot stress method provides less conservative estimates of the fatigue strength for the studied detail,  
3 together with lower scatter within the population of examined SN-curve data. Our confidence level on  
4 the applicability of the hot spot stress method on the investigated duplex specimen was supported by  
5 comparing the measured stress concentration factors – using strain gauges and digital image correlation  
6 – with the computed ones through finite element models – which show very consistent results.

7 A larger database of fatigue test results is then compiled for three details pertinent to bridge  
8 applications to emphasize the adequacy of the present European and IIW regulations to predict fatigue  
9 of higher strength steels details, namely transverse stiffeners, butt welds and cope holes. Then, using  
10 finite element analyses, each database is examined again at the nominal stress and hot spot stress  
11 ranges. This demonstrates the applicability of the hot spot stress method to a wider range of high  
12 strength steels. On the one hand, it is evident that the existing detail category or fatigue class is  
13 unconservative for cope holes and still excessively conservative for transverse stiffeners and butt  
14 welds. To make the current fatigue design rules for these detail categories more effective, suggestions  
15 are provided to upgrade the detail categories –  $FAT_k$  of transverse stiffeners and butt welds from 80 to  
16 90 MPa. This proposal is strengthened by a reliability analysis using the conventional two-parameter  
17 Weibull distribution. However, it is subsequently demonstrated that, throughout the entire range of  
18 grades considered in the database, the hot spot stress method generally provides more representative  
19 estimates with lower scatter.

## 20 **Acknowledgements**

21 We would like to gratefully acknowledge Research Foundation Flanders (FWO) for funding the first  
22 author for the post-doctoral project “1256522N”, and Outokumpu for providing plates made of EN  
23 1.4162 grade to be used in this research.

## 24 **References**

- 25 [1] W. Cui, Review article A state-of-the-art review on fatigue life prediction methods for, J Mar Sci Technol. (2002)  
26 43–56.
- 27 [2] G. Alencar, A. de Jesus, J.G.S. da Silva, R. Calçada, Fatigue cracking of welded railway bridges: A review, Eng  
28 Fail Anal. 104 (2019) 154–176. <https://doi.org/10.1016/j.engfailanal.2019.05.037>.



- [3] J.J. Duga, W.H. Fisher, R.W. Buxbaum, A.R. Rosenfield, A.R. Buhr, E.J. Honton, S.C. McMillan, The Economic Effects of Fracture in the United States Part 2 — A Report to NBS by Battelle Columbus Laboratories, National Bureau of Standards, 1983.
- [4] ASCE, Fatigue Reliability: Introduction, Journal of the Structural Division. 108 (1982) 3–23.
- [5] W. Schütz, A history of fatigue, Eng Fract Mech. 54 (1996) 263–300. [https://doi.org/10.1016/0013-7944\(95\)00178-6](https://doi.org/10.1016/0013-7944(95)00178-6).
- [6] X.W. Ye, Y.H. Su, J.P. Han, A state-of-the-art review on fatigue life assessment of steel bridges, Math Probl Eng. 2014 (2014). <https://doi.org/10.1155/2014/956473>.
- [7] R.P. Reed, J.H. Smith, B.W. Christ, The economic effects of fracture in the United States Part 1 — A Synopsis of the September 30, 1982 Report to NBS by Battelle Columbus Laboratories, National Bureau of Standards Special Publication, 1983.
- [8] A. Nussbaumer, L. Borges, Davaine L., Fatigue Design of Steel and Composite Structures, 1st ed., ECCS – European Convention for Constructional Steelwork, 2011.
- [9] ECCS TC6 working group, From Assessment to Best Practice A Collection of Historical Fatigue Damage Cases in Steel and Composite Bridges, 1st edition, No: 139, The European Convention for Constructional Steelwork (ECCS), 2020.
- [10] EN 1993-1-9, European Committee for Standardization, 2005. EN 1993-1-9, Eurocode 9: Design of steel structures - Part 1-9: Fatigue., CEN, Brussels., 2005.
- [11] EN 1993-1-10, European Committee for Standardization, 2005. EN 1993-1-10, Eurocode 3: Design of steel structures - Part 1-10: Material toughness and through-thickness properties., CEN, Brussels., 2005.
- [12] ECCS TC6 working group, Background Information on Fatigue Design Rules Statistical Evaluation, 2nd Edition, No: 140, The European Convention for Constructional Steelwork (ECCS), 2018.
- [13] C.M. Branco, S.J. Maddox, C.M. Sonsino, Fatigue design of welded stainless steels, European Commission, 2001.
- [14] A. Galtier, E.S. Statnikov, The influence of ultrasonic impact treatment on fatigue behaviour of welded joints in high-strength steel, Welding in the World. 48 (2004) 61–66. <https://doi.org/10.1007/BF03266433>.
- [15] A.M. Habraken, L. Duchêne, C. Bouffieux, U. Kuhlmann, A. Zizza, S. Breunig, V. Pourostad, L. Da Silva, C. Rebelo, H. Gervasio, C. Rigueiro, F. Maas, T. Baaten, B. Driesbeke, A. Reis, J. Pedro, C. Baptista, F. Virtuoso, C. Vieira, J.J. Dufrane, A.C. Vanderbecq, P. Toussaint, Optimal use of High Strength Steel grades within bridge (OPTIBRI), European Commission, 2019. <https://doi.org/10.2777/93807>.
- [16] P.J. Haagenzen, IIW's round robin and design recommendations for improvement methods, in: IIW Conference on Performance of Dynamically Loaded Welded Structures, San Francisco, 1997.
- [17] B. Karabulut, G. Lombaert, D. Debruyne, B. Rossi, Experimental and numerical fatigue assessment of duplex welded transversal stiffeners, 2020. <https://doi.org/10.1016/j.ijfatigue.2020.105498>.
- [18] O. Lagerqvist, M. Clarin, J. Gozzi, B. Völling, D. Pak, J. Stötz, H. Lieurade, B. Depale, I. Huther, S. Herion, J. Bergers, R. Martsch, M. Carlsson, A. Samuelsson, C. Sonander, Efficient lifting equipment with extra high-strength steel, European Commission, Research Fund for Coal and Steel (RFCS), 2007.
- [19] M. Liljas, C. Ericsson, Fatigue behaviour of stainless steel welds, in: AvestaPolarit Corrosion Management and Application Engineering, 2002.
- [20] M.M. Pedersen, O. Mouritsen, M.R. Hansen, J.G. Andersen, J. Wenderby, Comparison of post-weld treatment of high-strength steel welded joints in medium cycle fatigue, Welding in the World. 54 (2010) 208–217. <https://doi.org/10.1007/BF03263506>.
- [21] E.S. Statnikov, V.O. Muktepavel, A. Blomqvist, Comparison of ultrasonic impact treatment (UIT) and other fatigue life improvement methods, Welding in the World. 46 (2002) 20–32.
- [22] J. Tajima, A. Okukawa, Y. Tanaka, Fatigue design criteria on Honshu-Shikoku suspension bridges, IABSE Congress Report = Rapport Du Congrès AIPC = IVBH Kongressbericht. 10 (1976). <https://doi.org/http://doi.org/10.5169/seals-10467> Nutzungsbedingungen.
- [23] V.I. Trufiakov, E.S. Statnikov, P.P. Mikheev, A.Z. Kuzmenko, The efficiency of ultrasonic impact treatment for improving the fatigue strength of welded joints, IIW Document. (1998).

- [24] G. Zilli, E. Maiorana, J. Peultier, A. Fanica, O. Hechler, T. Rauert, R. Maquoi, Application of duplex stainless steel for welded bridge construction in an aggressive environment, European Commission, Research Fund for Coal and Steel (RFCS), 2008.
- [25] N.R. Baddoo, Stainless steel in construction: A review of research, applications, challenges and opportunities, *J Constr Steel Res.* 64 (2008) 1199–1206. <https://doi.org/10.1016/j.jcsr.2008.07.011>.
- [26] R. Merello, F.J. Botana, J. Botella, M.V. Matres, M. Marcos, Influence of chemical composition on the pitting corrosion resistance of non-standard low-Ni high-Mn–N duplex stainless steels, *Corros Sci.* 45 (2003) 909–921. [https://doi.org/10.1016/S0010-938X\(02\)00154-3](https://doi.org/10.1016/S0010-938X(02)00154-3).
- [27] A.K. Iversen, Stainless steels in bipolar plates-Surface resistive properties of corrosion resistant steel grades during current loads, *Corros Sci.* 48 (2006) 1036–1058. <https://doi.org/10.1016/j.corsci.2005.05.012>.
- [28] J. Olsson, M. Snis, Duplex - A new generation of stainless steels for desalination plants, *Desalination.* 205 (2007) 104–113. <https://doi.org/10.1016/j.desal.2006.02.051>.
- [29] Z. Wei, J. Laizhu, H. Jincheng, S. Hongmei, Study of mechanical and corrosion properties of a Fe-21.4Cr-6Mn-1.5Ni-0.24N-0.6Mo duplex stainless steel, *Materials Science and Engineering A.* 497 (2008) 501–504. <https://doi.org/10.1016/j.msea.2008.07.062>.
- [30] B. Burgan, N. Baddoo, L. Gardner, J. Way, B. Johansson, A. Olssen, E. Selen, R. Viherma, J. Kouhi, A. Talja, Development of the use of stainless steel in construction, European Commission, 2001.
- [31] C. Ericsson, P. Johansson, M. Liljas, E.M. Westin, Mechanical Properties of Welds in the New Lean Duplex Stainless Steel LDX 2101® (EN 1.4162, UNS S32101), in: *Stainless Steel World*, The Hague, 2003.
- [32] Y. Peng, J. Chen, J. Dong, Experimental data assessment and fatigue design recommendation for stainless-steel welded joints, *Metals (Basel).* 9 (2019). <https://doi.org/10.3390/met9070723>.
- [33] R. Strubbia, S. Hereñú, M.C. Marinelli, I. Alvarez-Armas, Fatigue damage in coarse-grained lean duplex stainless steels, *Materials Science and Engineering A.* 659 (2016) 47–54. <https://doi.org/10.1016/j.msea.2016.02.012>.
- [34] R. Strubbia, S. Hereñú, G. Gómez-Rosas, V. Fuster, C. Rubio González, Fatigue Life Improvement in Lean Duplex Stainless Steel by Peening Treatments, *Metall Mater Trans A Phys Metall Mater Sci.* 50 (2019) 5614–5626. <https://doi.org/10.1007/s11661-019-05455-y>.
- [35] N.R. Baddoo, A. Kosmac, Sustainable duplex stainless steel bridges, *Duplex 2010.* (2010).
- [36] M. Al-Emrani, R. Kliger, Fatigue prone details in steel bridges, in: *Nordic Steel Construction Conference 2009*, Malmö, Sweden, 2009: pp. 112–119.
- [37] R. Haghani, M. Al-emrani, M. Heshmati, Fatigue-Prone Details in Steel Bridges, (2012) 456–476. <https://doi.org/10.3390/buildings2040456>.
- [38] J.J.O. Pedro, A.J. Reis, C. Baptista, High strength steel (HSS) S690 in highway bridges: Comparative design, in: *Eurosteel 2017, EUROSTEEL 2017, Ernst and Sohn A Wiley Brand*, Copenhagen, 2017: pp. 4059–4068. <https://doi.org/10.1002/cepa.462>.
- [39] J.J.O. Pedro, A.J. Reis, C. Baptista, High Strength Steel S690 in highway bridges: General guidelines for design, *Stahlbau.* 87 (2018) 555–564. <https://doi.org/10.1002/stab.201810615>.
- [40] B. Karabulut, B. Rossi, G. Lombaert, Fatigue behaviour of duplex welded details, *KU Leuven*, 2021.
- [41] B. Karabulut, B. Rossi, On the fatigue behavior of duplex and high-strength welded cruciform joints, *Eng Struct.* 247 (2021) 113161. <https://doi.org/10.1016/j.engstruct.2021.113161>.
- [42] DMSSS, Euro Inox/SCI, 2017. Design manual for structural stainless steel., 4th ed., Euro Inox and the Steel Construction Institute, 2017.
- [43] EN ISO 6892-1, International Organization for Standardization, 2016. EN ISO 6892-1, Metallic materials — Tensile testing — Part 1: Method of test at room temperature, (2016).
- [44] M. Fortan, A. Dejans, B. Karabulut, D. Debruyne, B. Rossi, On the strength of stainless steel fillet welds, *J Constr Steel Res.* 170 (2020). <https://doi.org/10.1016/j.jcsr.2020.106081>.
- [45] M. Theofanous, L. Gardner, Experimental and numerical studies of lean duplex stainless steel beams, *J Constr Steel Res.* 66 (2010) 816–825. <https://doi.org/10.1016/J.JCSR.2010.01.012>.

- 1 [46] ASTM E 466 - 96, American Society for Testing and Materials, 2002. ASTM E466 - 96, Standard Practice for  
2 Conducting Force Controlled Constant Amplitude Axial Fatigue Tests of Metallic Materials, 2002.  
3 <https://doi.org/10.1520/E0466-96>.
- 4 [47] EN ISO 12106, International Organization for Standardization, 2017. Metallic materials — Fatigue testing —  
5 Axial-strain- controlled method, (2017).
- 6 [48] EN ISO 1099, International Organization for Standardization, 2017. Metallic materials — Fatigue testing — Axial  
7 force-controlled method, (2017).
- 8 [49] S.J. (Stephen J. Maddox, Fatigue strength of welded structures, (1991) 198.
- 9 [50] E. Niemi, W. Fricke, S.J. Maddox, Structural Hot-Spot Stress Approach to Fatigue Analysis of Welded  
10 Components, Springer Singapore, 2018. <https://doi.org/10.1007/978-981-10-5568-3>.
- 11 [51] A.F. Hobbacher, Recommendations for Fatigue Design of Welded Joints and Components, 2nd ed., International  
12 Institute of Welding (IIW), Springer International Publishing, 2016. <https://doi.org/10.1007/978-3-319-23757-2>.
- 13 [52] D.J. Kotecki, Some pitfalls in welding of duplex stainless steels, Soldagem & Inspeção. 15 (2010) 336–343.
- 14 [53] EN ISO 5817, International Organization for Standardization, 2016. EN ISO 5817, Welding - Fusion-welded joints  
15 in steel, nickel, titanium and their alloys (beam welding excluded) - Quality levels for imperfections (ISO  
16 5817:2014), 2014.
- 17 [54] V. Gunaraj, N. Murugan, Prediction of heat-affected zone characteristics in submerged arc welding of structural  
18 steel pipes, Welding Journal-New York-. 81 (2002) 45-s.
- 19 [55] N. Bailey, 1 - Factors influencing weldability, in: N. Bailey (Ed.), Weldability of Ferritic Steels, Woodhead  
20 Publishing, 1994: pp. 1–44. <https://doi.org/https://doi.org/10.1533/9781845698935.1>.
- 21 [56] EN ISO 9015-1, International Organization for Standardization, 2001. EN ISO 9015-1, Destructive tests on welds  
22 in metallic materials — Hardness testing — Part 1: Hardness test on arc welded joints, (2001).
- 23 [57] B. Karabulut, G. Ferraz, B. Rossi, Lifecycle cost assessment of high strength carbon and stainless steel girder  
24 bridges, J Environ Manage. 277 (2021) 111460. <https://doi.org/10.1016/j.jenvman.2020.111460>.
- 25 [58] B. Karabulut, B. Rossi, On the applicability of the hot spot stress method to high strength duplex and carbon steel  
26 welded details, Eng Fail Anal. 128 (2021) 105629. <https://doi.org/10.1016/j.engfailanal.2021.105629>.
- 27 [59] K. Shimizu, F. Sakata, Effect of Rolling Direction on Fatigue Crack Propagation in Pure Titanium Film, 66 (2017)  
28 921–927.
- 29 [60] W.R. Tyfour, J.H. Beynon, The effect of rolling direction reversal on fatigue crack morphology and propagation,  
30 Tribol Int. 27 (1994) 273–282. [https://doi.org/10.1016/0301-679X\(94\)90007-8](https://doi.org/10.1016/0301-679X(94)90007-8).
- 31 [61] E. Niemi, W. Fricke, S.J. Maddox, Fatigue Analysis of Welded Components Designer's guide to the structural hot-  
32 spot stress approach (IIW-1430-00), The International Institute of Welding (IIW), 2006.  
33 <https://doi.org/10.1017/CBO9781107415324.004>.
- 34 [62] DNV-RPC203, Det Norske Veritas AS, 2011. DNV-RPC203, Fatigue Design of Offshore Steel Structures., 2011.
- 35 [63] M.M. Pedersen, O.O. Mouritsen, M.R. Hansen, J.G. Andersen, J. Wenderby, Re-analysis of fatigue data for welded  
36 joints using the notch stress approach, Int J Fatigue. 32 (2010) 1620–1626.  
37 <https://doi.org/10.1016/j.ijfatigue.2010.03.001>.
- 38 [64] A. Ohta, Y. Maeda, N. Suzuki, Residual stress effect on fatigue strength of non-load-carrying cruciform welded  
39 joints of SM570Q steel for welded structures, Welding in the World. 46 (2002) 20–25.  
40 <https://doi.org/10.1007/BF03263393>.
- 41 [65] C. Sonander, Ermüdung von geschweißten Kreuzstößen aus WELDOX 1100, Stahlbau. 69 (2000) 317–322.  
42 <https://doi.org/10.1002/stab.200000930>.
- 43 [66] J.D.M. Costa, J.A.M. Ferreira, L.P.M. Abreu, Fatigue behaviour of butt welded joints in a high strength steel,  
44 Procedia Eng. 2 (2010) 697–705. <https://doi.org/10.1016/j.proeng.2010.03.075>.
- 45 [67] M. Koskimaki, E. Niemi, Fatigue strength of polarit 721, 803 and 854 welded joints, in: H. Nordberg, J. Björklund  
46 (Eds.), Application of Stainless Steel '92, Stockholm, 1993: pp. 889–898.
- 47 [68] T. McGoughy, Fatigue of stainless steel weldments, in: EWI Research Report, IIW Document XII-1768-99, 1994.

- [69] T. Wang, D. Wang, L. Huo, Y. Zhang, Discussion on fatigue design of welded joints enhanced by ultrasonic peening treatment (UPT), *Int J Fatigue*. 31 (2009) 644–650. <https://doi.org/10.1016/j.ijfatigue.2008.03.030>.
- [70] C. Miki, K. Tateishi, Fatigue strength of cope hole details in steel bridges, *Int J Fatigue*. 19 (1997) 445–455. [https://doi.org/10.1016/S0142-1123\(97\)85727-1](https://doi.org/10.1016/S0142-1123(97)85727-1).
- [71] M. Aygöl, M. Al-Emrani, S. Urushadze, Modelling and fatigue life assessment of orthotropic bridge deck details using FEM, *Int J Fatigue*. 40 (2012) 129–142. <https://doi.org/10.1016/j.ijfatigue.2011.12.015>.
- [72] M. Heshmati, Fatigue life assessment of bridge details using finite element method, Chalmers University of Technology, 2012.
- [73] M. Heshmati, M. Al-Emrani, Fatigue design of plated structures using structural hot spot stress approach, in: *Proceedings of the Sixth International Conference on Bridge Maintenance, Safety and Management, IABMAS 2012*, Stresa, Lake Maggiore, 8-12 July 2012, 2012: pp. 3146–3153.
- [74] X. Wei, L. Xiao, S. Pei, Fatigue assessment and stress analysis of cope-hole details in welded joints of steel truss bridge, *Int J Fatigue*. 100 (2017) 136–147. <https://doi.org/10.1016/j.ijfatigue.2017.03.032>.
- [75] P. Liao, B. Qu, Y. Huang, Y. Jia, Y. Wang, H. Zhu, Fatigue life assessment of revised cope-hole details in steel truss bridges, *Metals (Basel)*. 10 (2020) 1–14. <https://doi.org/10.3390/met10081092>.
- [76] Z.G. Xiao, K. Yamada, Fatigue Strength of Intersecting Attachments, *Journal of Structural Engineering*. 131 (2005) 946–955. <https://doi.org/10.1061/共ASCE733-9445共2005733:6共924733 CE>.
- [77] B. Waloddi Weibull, A Statistical Distribution Function of Wide Applicability, *J Appl Mech*. 18 (1951) 293–297. <https://doi.org/10.1115/1.4010337>.
- [78] J.C. Fothergill, Estimating the Cumulative Probability of Failure Data Points to be Plotted on Weibull and other Probability Paper, *IEEE Transactions on Electrical Insulation*. 25 (1990) 489–492. <https://doi.org/10.1109/14.55721>.
- [79] L. Goglio, M. Rossetto, Comparison of fatigue data using the maximum likelihood method, *Eng Fract Mech*. 71 (2004) 725–736. [https://doi.org/10.1016/S0013-7944\(03\)00009-2](https://doi.org/10.1016/S0013-7944(03)00009-2).
- [80] Bolfarine Heleno, Sandoval Monica Carneiro, Introduction to the statistical inference [In Portuguese], Sao Paulo, 2000. [https://docs.ufpr.br/~lucambio/CE085/IS2017/LIVRO\\_Bolfarine\\_Sandoval.pdf](https://docs.ufpr.br/~lucambio/CE085/IS2017/LIVRO_Bolfarine_Sandoval.pdf) (accessed February 20, 2023).
- [81] J.F. Barbosa, R. Carlos Silverio Freire Júnior, J.A.F.O. Correia, A.M.P. de Jesus, R.A.B. Calçada, Analysis of the fatigue life estimators of the materials using small samples, <https://doi.org/10.1177/0309324718782245>. 53 (2018) 699–710. <https://doi.org/10.1177/0309324718782245>.
- [82] L.F. Zhang, M. Xie, L.C. Tang, On weighted least squares estimation for the parameters of Weibull distribution, *Springer Series in Reliability Engineering*. 18 (2008) 57–84. [https://doi.org/10.1007/978-1-84800-113-8\\_3/COVER](https://doi.org/10.1007/978-1-84800-113-8_3/COVER).
- [83] B. Pedrosa, J.A.F.O. Correia, C.A.S. Rebelo, M. Veljkovic, Reliability of Fatigue Strength Curves for Riveted Connections Using Normal and Weibull Distribution Functions, *ASCE ASME J Risk Uncertain Eng Syst A Civ Eng*. 6 (2020). <https://doi.org/10.1061/ajrua6.0001081>.
- [84] D.D.J. Smith, Variable Failure Rates and Probability Plotting, *Reliability, Maintainability and Risk*. (2022) 75–87. <https://doi.org/10.1016/B978-0-323-91261-7.00006-X>.
- [85] Y. Bai, W.-L. Jin, Reliability-Based Design and Code Calibration, *Marine Structural Design*. (2016) 645–670. <https://doi.org/10.1016/B978-0-08-099997-5.00035-6>.